Merge Now, Regret Later: The Hidden Cost of Model Merging is Adversarial Transferability

Ankit Gangwal, Aaryan Ajay Sharma International Institute of Information Technology, Hyderabad, India gangwal@iiit.ac.in, aaryan.s@research.iiit.ac.in

Abstract—Model Merging (MM) has emerged as a promising alternative to multi-task learning, where multiple fine-tuned models are combined, without access to tasks' training data, into a single model that maintains performance across tasks. Recent works have explored the impact of MM on adversarial attacks, particularly backdoor attacks. However, none of them have sufficiently explored its impact on transfer attacks using adversarial examples, i.e., a black-box adversarial attack where examples generated for a surrogate model successfully mislead a target model.

In this work, we study the effect of MM on the transferability of adversarial examples. We perform comprehensive evaluations and statistical analysis consisting of 8 MM methods, 7 datasets, and 6 attack methods, sweeping over 336 distinct attack settings. Through it, we first challenge the prevailing notion of MM conferring free adversarial robustness, and show MM cannot reliably defend against transfer attacks, with over 95% relative transfer attack success rate. Moreover, we reveal 3 key insights for machine-learning practitioners regarding MM and transferability for a robust system design: (1) stronger MM methods increase vulnerability to transfer attacks; (2) mitigating representation bias increases vulnerability to transfer attacks; and (3) weight averaging, despite being the weakest MM method, is the most vulnerable MM method to transfer attacks. Finally, we analyze the underlying reasons for this increased vulnerability, and provide potential solutions to the problem. Our findings offer critical insights for designing more secure systems employing MM.

I. INTRODUCTION

Pre-Trained Models (PTMs) are becoming increasingly popular across various domains, ranging from image recognition to natural language processing [1], [2], [3], [4], [5]. They offer powerful representations that can be adapted to various downstream tasks through fine-tuning. However, fine-tuning often leads to degradation of multi-task performance, i.e., tasks other than the one being optimized [6]. To counteract this issue, Model Merging (MM) [7], [8], [9], [10], [11] has recently emerged as a promising alternative, with over 30,000 merged models on HuggingFace [12]. MM enables combining multiple fine-tuned models into a single model that retains or even enhances performance across multiple tasks, without training or access to task-specific data.

Despite its growing popularity, the security of MM methods remains largely unexplored. Recent research has shown that MM can mitigate certain types of adversarial attacks. Specifically, Arora et al. [13] demonstrated that merging a backdoored model with benign models can neutralize the backdoor, effectively sanitizing the merged model and appearing to provide a "free lunch" of adversarial robustness.

However, in this work, we challenge this prevailing notion by showing that while MM may mitigate backdoor attacks, it actually increases vulnerability to another class of adversarial threats: (transferable) adversarial examples, which are subtly modified inputs that can mislead models into making incorrect predictions [14]. These examples also exhibit the property of transferability [15], i.e., the tendency to remain effective even on models trained with different datasets or with different architecture, so long as both models perform the same task. This enables an adversary to launch a transfer attack, where an adversarial example crafted on a surrogate model can successfully mislead a target model, even without access to its parameters or architecture [16].

Existing literature on adversarial transferability suggests adversarial examples tend to transfer well between models having same architecture [17]. Therefore, in order to evade a Machine Learning as a Service (MLaaS) system that internally employs a merged model, an adversary can use as the surrogate either (1) the publicly available PTM that shares the same architecture with the merged model, or (2) one of the fine-tuned models that was used in the merged model's MM process, and expect the transfer attack to succeed with high probability. Figure 1 illustrates a possible attack strategy of adversary.

Beyond this apparent threat, it also remains unclear how the strength of the MM method affects the risk of transferability, or whether certain MM methods are particularly vulnerable to transfer attacks. To our best knowledge, none of the existing works have extensively studied the relation between transferable adversarial examples and MM. Therefore, we study MM under this threat model, find several statistically validated empirical results that challenge the status quo and take the following position:

Position: MM does not confer free adversarial robustness; rather, it comes at the hidden cost of (increased) threat to adversarial example based transfer attacks.

We further give explanations for our findings and discuss potential solutions to address this problem.

Contribution: The major contributions of our work are:

1) We challenge the prevailing notion of MM giving free adversarial robustness, by showing it is vulnerable to

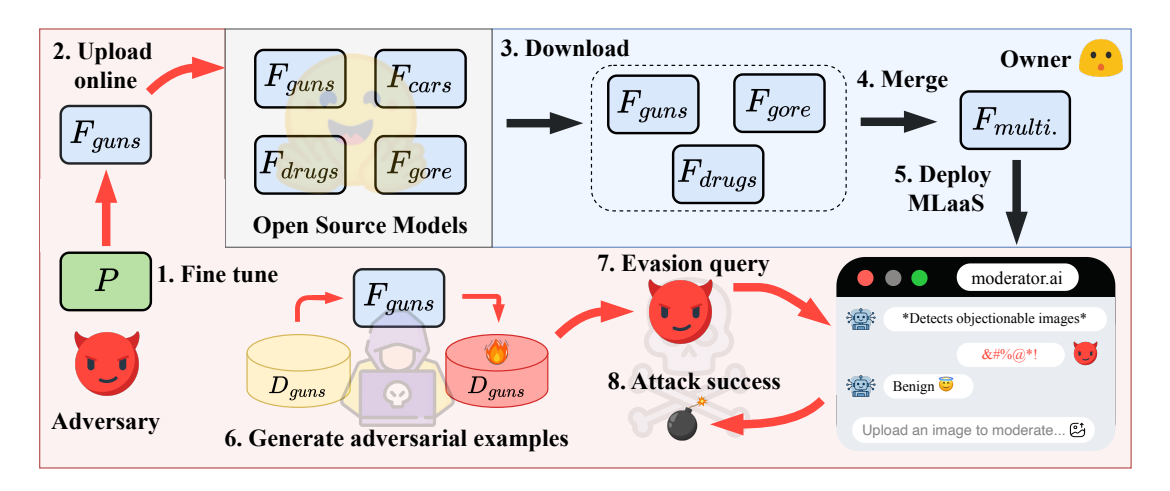


Fig. 1. Illustration of a possible attack strategy of adversary. (1) Adversary fine-tunes the PTM for classifying objectionable content (Guns) and (2) uploads it online on open-source platforms like HuggingFace. (3) The owner (victim) downloads multiple models fine-tuned to classify objectionable contents (e.g., guns, drugs, gore) and (4) merges them into a single model. (5) Owner then deploys the merged model as an MLaaS. (6) Adversary then generates adversarial examples using either the previously uploaded fine-tune model or off-the-shelf PTM as surrogate and (6) launches an evasion attack on owner's MLaaS. Finally, due to architectural or decision boundary similarity between surrogate and target model, (7) the attack succeeds.

transfer attacks, with a relative transfer Attack Success Rate (ASR) exceeding 95% (cf. §V).

- 2) We statistically validate our empirical results in more than 336 different attack settings (8 MM methods, 7 datasets, 6 attack methods) and arrive at 3 key findings:
 - a) Stronger MM method increases the risk of transfer attacks (cf. §V-A).
 - b) Reducing representation bias increases the risk of transfer attacks (cf. §V-B).
 - c) As a method-specific finding, we observe that weight averaging is most vulnerable to transfer attacks, despite being the weakest MM methods (cf. §V-C).
- 3) We explain the reasons for each of our findings, and give a potential solution for robust MM (cf. §VII).

Organization: The remainder of this paper is organized as follows. §II presents the relevant background knowledge for paper. We elucidate our threat model in §III. §IV details our experimental setup, followed by evaluation results in §V. §VI summarizes related works. §VII discusses explanation of findings, solutions and other results, and §VIII concludes.

II. BACKGROUND

Notations. Let $f_{\boldsymbol{\theta}}: \mathbb{R}^D \to [0,1]^c$ denote an image classification neural network model parameterized by the vector $\boldsymbol{\theta} \in \mathbb{R}^n$. The input is a vector $\mathbf{x}_i \in \mathbb{R}^D$, and the model outputs a probability distribution over c classes: $\hat{\mathbf{y}}_i = f_{\boldsymbol{\theta}}(\mathbf{x}_i) = [\hat{y}_{i,1}, \dots, \hat{y}_{i,c}]^\top \in [0,1]^c$, with $\sum_{j=1}^c \hat{y}_{i,j} = 1$. Given a dataset $\mathcal{D}_{tr} = \{(\mathbf{x}_i, \mathbf{y}_i)\}_{i=1}^{N_{tr}}$, the ground truth label $\mathbf{y}_i \in \{0,1\}^c$ is represented in one-hot encoding. The model predicts label (class index) $\arg\max_j \hat{y}_{i,j}$. Here, n denotes the number of parameters, D is the input dimension, $N_{tr} = |\mathcal{D}_{tr}|$ is the number of training samples, and c is the number of output classes. TABLE I summarizes the notation used in our work.

TABLE I
A SUMMARY OF THE NOTATIONS USED IN OUR WORK.

Notation	Description	Notation	Description
t	tth fine-tuning task	t_{γ}	Number of iterations for γ
\mathcal{D}_{tr}^t	Training dataset	t_s	Test statistic for t-test
$T_{te}^{t'}$	Test dataset	W	Test statistic for Wilcoxon test
T	Total number of tasks	d	Cohen's d
m	MM method	r	Wilcoxon's r
\mathcal{M}	Space of MM methods	α_{γ}	Step size for γ
x	Clean input	$\epsilon^{'}$	Perturbation budget
$\tilde{\mathbf{x}}$	Perturbed input	Ø	Null set
γ	Attack method	Δ	ASR difference
Γ	Space of attack methods	Δ	ASR difference tensor
\mathbf{A}_{γ}^{t}	Transfer ASR matrix for γ , t	Å	ASR difference set
$\overline{R}_{\gamma}^{t,s}$	Mean relative transfer ASR for γ , t	Q_e	False discovery rate
μ	Mean	[n]	$\{1,, n\}$
$\mu_{1/2}$	Median	α	Significance level

A. Model Merging

Consider T independently fine-tuned models $\{f_{\theta_t}\}_{t=1}^T$, each trained on its own, task-specific dataset $\mathcal{D}_{tr}^t \subseteq \mathbb{R}^D \times \{0,1\}^c$. Following prior work [11], we assume all f_{θ_t} are fine-tuned from a common pre-trained backbone f_{θ_0} (e.g., ViT [3], ResNet [4]). MM aims to combine the parameter vectors $\{\theta_t\}_{t=1}^T$ of T independently fine-tuned models into a single parameter vector $\boldsymbol{\theta}_{mtl}^m$, such that the resulting model $f_{\boldsymbol{\theta}_{mtl}^m}$ can simultaneously perform well on all tasks $t \in [T]$. Mathematically, $\zeta_m : \mathbb{R}^{n \times T} \to \mathbb{R}^n$ such that $\zeta_m(\boldsymbol{\Theta}) = \boldsymbol{\theta}_{mtl}^m$, where $\boldsymbol{\Theta} = [\theta_1 \ \theta_2 \ \cdots \ \theta_T] \in \mathbb{R}^{n \times T}$ is combined parameter matrix, ζ_m is the function performing MM and m denotes a specific merging method.

A key constraint for MM is that access to the task-specific fine-tuning data $\{\mathcal{D}^t_{tr}\}_{t=1}^T$ is restricted during the merging process. The objective therefore, is to minimize the average loss of the merged model across all task-specific test sets $\{\mathcal{D}^t_{te}\}_{t=1}^T$, where each test set contains labeled pairs $(\mathbf{x}_i, \mathbf{y}_i) \in$

 $\mathbb{R}^D \times \{0,1\}^c$. Formally, the optimization goal is:

$$\min_{\boldsymbol{\theta}_{mtl}^{m}} \frac{1}{T} \sum_{t=1}^{T} \frac{1}{|\mathcal{D}_{te}^{t}|} \sum_{i=1}^{|\mathcal{D}_{te}^{t}|} \mathcal{L}(f_{\boldsymbol{\theta}_{mtl}^{m}}(\mathbf{x}_{i}), \mathbf{y}_{i}), \tag{1}$$

where $\mathcal{L}(\cdot)$ is a task-specific loss function, such as the cross-entropy loss.

We discuss four representative *pre-hoc* MM methods (i.e., operating to obtain θ^m_{mtl}) and one *post-hoc* MM method (i.e., operating after θ^m_{mtl} is obtained) considered in our work below:

1) Weight Averaging (WA) [7]. The simplest merging strategy is WA, which directly averages the parameter vectors $\{\theta_t\}_{t=1}^T$ from multiple fine-tuned models:

$$\boldsymbol{\theta}_{mtl}^{\text{WA}} = \frac{1}{T} \sum_{t=1}^{T} \boldsymbol{\theta}_{t}.$$
 (2)

However, this simple averaging often leads to suboptimal performance across tasks.

2) Task Arithmetic (TA) [8]. TA defines a task vector τ_t by subtracting the pre-trained parameter vector θ_0 from each fine-tuned model's parameter vector θ_t , i.e., $\tau_t = \theta_t - \theta_0$. These task vectors $\{\tau_t\}_{t=1}^T$ are aggregated and added back to the PTM as:

$$\boldsymbol{\theta}_{mtl}^{\text{TA}} = \boldsymbol{\theta}_0 + \lambda \sum_{t=1}^{T} \boldsymbol{\tau}_t, \tag{3}$$

where $\lambda \in \mathbb{R}$ is the scaling coefficient, which is a hyper-parameter that can be tuned to control the contribution of the task vectors.

3) **TIES-Merging (TM) [9].** Building on the task vector formulation, TM introduces a refinement process to address the issue of interference and sign conflicts in $\{\tau_t\}_{t=1}^T$. It applies three operations — TRIM, ELECT SIGN, and MERGE — collectively on $\{\tau_t\}_{t=1}^T$. Let $\Psi(\tau_t)$ denote t^{th} task vector after applying the three operation. The final merged model is then computed as:

$$\boldsymbol{\theta}_{mtl}^{\text{TM}} = \boldsymbol{\theta}_0 + \lambda \sum_{t=1}^{T} \Psi(\boldsymbol{\tau}_t).$$
 (4)

4) **AdaMerging (AM) [10].** AM extends this approach by adaptively learning task-specific or layer-specific scaling coefficients. In task-wise AM, the merged model is given by:

$$\boldsymbol{\theta}_{mtl}^{\text{AM}} = \boldsymbol{\theta}_0 + \sum_{t=1}^{T} \lambda_t \boldsymbol{\tau}_t, \tag{5}$$

where $\lambda_t \in \mathbb{R}$ is the scaling coefficient that is learned per task t. For layer-wise AM, the model is merged per layer $l \in [L]$ as:

$$\boldsymbol{\theta}_{mtl}^{\text{AM}} = \left\{ \boldsymbol{\theta}_0^l + \sum_{t=1}^T \lambda_t^l \boldsymbol{\tau}_t^l \right\}_{l=1}^L, \tag{6}$$

where L is the total number of layers in the model, and θ_0^l , τ_t^l , and λ_t^l denote the layer-wise parameters,

layer-wise task vectors, and layer-wise learned scaling coefficients, respectively.

Representation Surgery (RS) [11]. RS is a post-hoc MM method, in the sense that it does not combine $\{\theta_t\}_{t=1}^T$ into θ_{mtl}^{m} . Rather, it first observes that both simple and advanced MM techniques often suffer from a representation bias—a consistent, task-specific discrepancy between the feature representations of the merged model and those of the individual fine-tuned models, and tries to mitigate this representation bias. To achieve this, RS introduces a task-specific adapter function $\Phi_t(\cdot)$ for each task $t \in [T]$, which aims to correct for the task-specific bias in the representation space. Let $Z_{mtl}^t \in \mathbb{R}^{|\mathcal{D}_{te}^t| \times k}$ and $Z_{ind}^t \in \mathbb{R}^{|\mathcal{D}_{te}^t| \times k}$ denote the feature matrices extracted from the merged model and the individual fine-tuned model respectively for task t, where k is the feature dimension. Each adapter is parameterized by θ_{Φ_t} and learns to estimate the representation bias via the transformation $\Phi_t(\boldsymbol{Z}_{mtl}^t)$. The goal is to minimize the average ℓ_1 distance between the feature representation of the merged model and the corresponding individual model features:

$$\arg\min_{\{\boldsymbol{\theta}_{\Phi_t}\}_{t=1}^T} \frac{1}{T} \sum_{t=1}^T \frac{1}{|\mathcal{D}_{te}^t|} \left\| \widehat{\boldsymbol{Z}}_{mtl}^t - \boldsymbol{Z}_{ind}^t \right\|_1, \quad (7)$$

subject to the constraint:

$$\widehat{\boldsymbol{Z}}_{mtl}^{t} = \boldsymbol{Z}_{mtl}^{t} - \Phi_{t}(\boldsymbol{Z}_{mtl}^{t}), \tag{8}$$

where \hat{Z}_{mtl}^t denotes the debiased representation for task t. Due to this post-hoc surgical removal of representation bias, RS can be combined with any pre-hoc MM methods (e.g., WA).

Following our previous discussion, let \mathcal{M} denote the space of MM methods considered in this work. Specifically, \mathcal{M} is defined as the Cartesian product of two sets: $\{WA, TA, TM, AM\}$, denoting four representative merging methods, and $\{\varnothing, RS\}$, indicating the absence or presence of RS, respectively, i.e., $\mathcal{M} = \{WA, TA, TM, AM\} \times \{\varnothing, RS\}$. Each merging method m considered in our study is an element of this space, i.e., $m \in \mathcal{M}$. For ease of notation, we shall refer to the method $m = (u, \varnothing)$ as simply u and m = (u, RS) as u + RS henceforth (e.g., $(WA, \varnothing) \mapsto WA$, $(WA, RS) \mapsto WA+RS$).

B. Adversarial Examples

Adversarial examples are perturbed inputs intentionally crafted to cause a trained neural network model to produce incorrect predictions, despite the perturbation being imperceptibly small to humans [14]. Formally, a valid adversarial example is a perturbed input $\tilde{\mathbf{x}}_i = \mathbf{x}_i + \boldsymbol{\delta}_i$ that satisfies the following properties [18], [19]:

• Bounded Perturbation. The perturbation vector $\delta_i \in \mathbb{R}^D$ is constrained such that $\|\delta_i\|_p \leq \epsilon$ where $\epsilon > 0$ is the perturbation budget and norm $\|\cdot\|_p$ (e.g., ℓ_{∞} , ℓ_{2}).

• **Prediction Change.** The model's predicted class on the adversarial example differs from the original prediction, i.e.,

$$\arg\max_{j} f_{\boldsymbol{\theta}}(\tilde{\mathbf{x}}_{i})_{j} \neq \arg\max_{j} f_{\boldsymbol{\theta}}(\mathbf{x}_{i})_{j}. \tag{9}$$

One of the surprising properties of adversarial examples is their transferability [16]—the phenomenon where an adversarial example $\tilde{\mathbf{x}}_i$ crafted to fool one model f_{θ} can also fool a different model $f_{\theta'}$, even if the second model has a different architecture, training data, or initialization, as long as they perform the same task. Formally, we say an adversarial example transfers from f_{θ} to $f_{\theta'}$, if it satisfies both Eq. (9) and Eq. (10) as follows:

$$\arg\max_{j} f_{\boldsymbol{\theta}'}(\tilde{\mathbf{x}}_{i})_{j} \neq \arg\max_{j} f_{\boldsymbol{\theta}'}(\mathbf{x}_{i})_{j}. \tag{10}$$

Transferability enables the feasibility of (black-box) transfer attacks, where an adversary crafts adversarial examples using a surrogate model f_{θ} and launches them against a target model $f_{\theta'}$ for evasion, without having access to its parameters or gradients. Several factors influence transferability, including model architecture similarity [20], alignment of decision boundaries [21], and the choice of attack method [15].

Various attack methods to generate adversarial examples have been proposed by optimizing the perturbation δ_i under norm constraints. We use the following five first-order attacks and one query-based black-box attack in our work: (1) Fast Gradient Sign Method (FGSM) [22]; (2) Iterative FGSM (I-FGSM) [23]; (3) Projected Gradient Descent (PGD) [24]; (4) Nesterov I-FGSM (NI-FGSM) [25]; (5) Translation-Invariant FGSM (TI-FGSM) [26]; and (6) Square Attack [27]. We describe them in detail in Appendix A.

Consequently, we define the space of attack methods Γ as $\{FGSM, I\text{-}FGSM, PGD, NI\text{-}FGSM, TI\text{-}FGSM\}^1$, with attack method γ being an element of this space, i.e., $\gamma \in \Gamma$.

III. THREAT MODEL

Actors. We have two actors in our threat model: (1) owner \mathcal{O} , who uses MM method $m \in \mathcal{M}$ for creating model $f_{\theta_{mtt}^m}$. \mathcal{O} employs $f_{\theta_{mtt}^m}$ in her system and makes it publicly available as an MLaaS via an API; and (2) adversary \mathcal{A} , which has illicit gains for evading/bypassing \mathcal{O} 's system.

Adversary's Goal. \mathcal{A} 's goal is make \mathcal{O} 's model $f_{\boldsymbol{\theta}_{mtl}^m}$ change its prediction on an input of interest \mathbf{x} . Formally, \mathcal{A} 's goal is finding $\tilde{\mathbf{x}} = \mathbf{x} + \boldsymbol{\delta}$ such that:

$$\arg\max_{j} f_{\boldsymbol{\theta}_{mtl}^{m}}(\tilde{\mathbf{x}})_{j} \neq \arg\max_{j} f_{\boldsymbol{\theta}_{mtl}^{m}}(\mathbf{x})_{j}, \tag{11}$$

with $|\delta|_p \leq \epsilon$. As a concrete example, \mathcal{O} 's MLaaS system can be an automatic image moderation service like PicPurify² or sightengine³, where \mathcal{A} 's illicit gain comes from evading such image moderation system.

Adversary's Capabilities. Following prior works on image-classification black-box adversarial attacks [26], [25], we consider an ℓ_{∞} -norm constrained threat model, i.e, $|\tilde{\mathbf{x}} - \mathbf{x}|_{\infty} \leq \epsilon$. This implies \mathcal{A} is capable of perturbing any pixel of the image by value at most ϵ . Unless otherwise stated, we assume \mathcal{A} performs untargeted transfer attack since they are harder to defend against, and since targeted transfer attacks, although practical, are much harder to perform [28]. We discuss the results on targeted attacks in §VII-C.

Adversary's Knowledge. We make three assumption regarding A's knowledge: (1) A knows O has used MM while creating her model; (2) A knows the specific architecture of the model being merged; (3) A has access to one of the two kinds of surrogate model (that is used by the \mathcal{O} while creating her merged model): (a) PTM f_{θ_0} or (b) fine-tuned model f_{θ_t} on task t, which she uses to craft transferable adversarial examples using attack method $\gamma \in \Gamma$. Assumption (3) is realistic in the scenario where \mathcal{O} builds her merged model by downloading off-the-shelf fine-tuned models, as illustrated in Fig. 1. However, we do consider the case where we let go of these three assumptions, i.e., where A performs the transfer attack with a surrogate of different architecture in §VII-E. Following previous works on MM [10], [11], we assume A, like \mathcal{O} , does not have access to any task-specific training data \mathcal{D}_{tr}^{t} , while having partial access to unlabeled task-specific test data \mathcal{D}_{te}^t .

IV. EXPERIMENTAL DETAILS

Experimental Setup. We run all our experiments on an NVIDIA DGX A100 machine using the PyTorch [29] framework, and use Adam [30] as the optimizer.

Datasets and Models. To capture diverse domains, we selected 7 image datasets: (t=1) Cars [31], (t=2) MNIST [32], (t=3) EuroSAT [33], (t=4) GTSRB [34], (t=5) SVHN [35], (t=6) RESISC45 [36] and (t=7) DTD [37], in accordance with previous work on MM [11]. Please refer to Appendix B-A for dataset description. Following prior works [11], we mainly use a CLIP model [5] with ViT-32/B [3] as the backbone for classification. We also use a CLIP model with ResNet-50 [38] backbone in \S VII-E. Model accuracies for each model considered in our work is given in TABLE II.

TABLE II
MODEL ACCURACIES (IN %) ON SEVEN TASKS.

Model \downarrow / t \rightarrow	Cars	MNIST	EuroSAT	GTSRB	SVHN	RESISC45	DTD	Avg.
Pretrained (ViT)	59.73	48.26	45.52	32.60	31.63	60.67	43.99	46.07
Pretrained (RN50)	57.01	61.08	33.59	36.14	33.81	54.11	43.19	45.56
Individual (ViT)	77.73	99.69	99.87	98.73	97.46	95.98	79.36	92.69
Individual (RN50)	75.99	99.57	97.59	98.78	96.77	93.35	67.50	89.94
WA	63.29	87.28	72.46	53.02	64.52	71.83	50.85	66.18
TA	58.13	97.37	80.81	72.43	81.42	69.13	52.50	73.11
TM	65.32	96.27	76.02	70.02	81.36	75.84	55.11	74.28
AM	67.91	99.44	87.74	75.72	86.42	78.84	57.29	79.05
WA+ RS	65.20	97.78	96.15	82.34	75.21	86.22	69.47	81.77
TA + RS	61.11	98.55	95.59	86.71	87.19	83.24	67.66	82.86
TM + RS	65.97	98.27	96.15	86.45	85.74	86.78	69.73	84.16
AM + RS	68.54	99.50	96.43	87.23	89.43	87.49	71.60	85.74

Attack Methods. For attack methods, we employ the standard FGSM [22] and the state-of-the-art method: NI-

 $^{^{1}}$ We exclude Square attack from Γ for notational convenience and uniformity when performing statistical analysis in $\S V$.

²https://www.picpurify.com/demo-gun.html

³https://sightengine.com/detect-weapons-alcohol-drugs

FGSM [25] and TI-FGSM [26], designed for black-box transfer settings. We also consider I-FGSM [23] and PGD [24], which are generally known to perform better in white-box settings, to provide additional context. Finally, to evaluate MM against query-based black-box attack, we employ Square Attack [27]. We split the test data into two disjoint halves, and use one half for evaluation of merged models and the other to generate adversarial examples. Please refer to Appendix B-B for attack hyperparameter details.

Metric. We use the ASR to measure the success of a transfer attack. ASR is defined as the proportion of test examples for which the top-1 prediction of the target model $f_{\theta'}$ on the adversarial input $\tilde{\mathbf{x}}_i$ differs from its prediction on the corresponding clean input \mathbf{x}_i [16]. Mathematically, we define ASR as:

$$\frac{1}{|\mathcal{D}_{te}^t|} \sum_{i=1}^{|\mathcal{D}_{te}^t|} \mathbb{I}\left(\arg\max_{j} f_{\boldsymbol{\theta}'}(\tilde{\mathbf{x}}_i)_j \neq \arg\max_{j} f_{\boldsymbol{\theta}'}(\mathbf{x}_i)_j\right), \tag{12}$$

where $\mathbb{I}(\cdot)$ is the indicator function.

V. EVALUATING TRANSFERABILITY IN MODEL MERGING
We first aim to find the answer to the following question:

How Successful is Model Merging in Defending Against Transfer Attacks? Specifically, to what extent does the success of A in transfer attacks differ from that in the white-box scenario?

To answer this, we formulate the problem as follows: for each task $t \in [T]$, and attack method $\gamma \in \Gamma$, define ASR matrix $\mathbf{A}_{\gamma}^t \in [0,1]^{|\mathcal{S}| \times |\mathcal{T}|}$, where rows correspond to surrogate models $\mathcal{S} = \{f_{\theta_0}, f_{\theta_t}\}$ and columns to target models $\mathcal{T} = \mathcal{S} \cup \{f_{\boldsymbol{\theta}_{mtt}^m} \mid m \in \mathcal{M}\}^4$. Each entry $[\mathbf{A}_{\gamma}^t]_{s,l}$ denotes the ASR obtained by generating adversarial examples on surrogate model $s \in \mathcal{S}$ and evaluating them on target model $l \in \mathcal{T}$. We quantify the success of transfer attack relative to its success in white-box setting by taking the average of target model

ASRs, and then normalizing by its corresponding white-box ASR. Mathematically, we define it as

$$\overline{R}_{\gamma}^{t,s} = \frac{1}{|\mathcal{T} \backslash \mathcal{S}|} \sum_{l \in \mathcal{T} \backslash \mathcal{S}} \frac{[\mathbf{A}_{\gamma}^{t}]_{s,l}}{[\mathbf{A}_{\gamma}^{t}]_{s,s}}, \tag{13}$$

where $\overline{R}_{\gamma}^{t,\,s}$ denotes mean relative transfer ASR for attack γ and task t, when transferring adversarial examples from surrogate s to all other target models $l\in\mathcal{T}\backslash\mathcal{S}$. For example, a higher value of $\overline{R}_{\gamma}^{t,\,s}=80\%$ would imply on an average, 80% of adversarial examples that succeed on the surrogate model also succeed when transferred to the target (merged) models and MM could not defend against transfer attack. Similarly, a lower value of $\overline{R}_{\gamma}^{t,\,s}=20\%$ would mean MM successfully defending transfer attack. Due to page limitations, we give the result of $\{\mathbf{A}_{\gamma}^t\}_{t=1}^T$ for the strongest performing attack method $\gamma=\mathrm{NI-FGSM}$ in TABLE III, and defer the results of $\{\mathbf{A}_{\gamma}^t\}_{t=1}^T$, $\forall\,\gamma\in\Gamma\backslash\{\mathrm{NI-FGSM}\}$ to Appendix E.

From TABLE III, we observe $\overline{R}_{\gamma}^{t,\,s} > 95\%$ in most (10/14) cases, with an average $\overline{R}_{\gamma}^{t,\,s}$ of 98.51%. We also see $\overline{R}_{\gamma}^{t,\,s}$ greater than 100% for (t=1) Cars, (t=3) EuroSAT and (t=7) DTD when $s=f_{\theta_0}$. This means in many cases, the white-box ASR was lesser than black-box ASR when using pretrained model as the surrogate. We conjecture this occurs due to f_{θ_0} 's lower accuracy on the task than f_{θ_1} and f_{θ_0} masking/obfuscating the gradients with noise [39]. Overall, we conclude the following:

Takeaway

Model Merging Cannot Defend Against Transfer Attacks. Therefore, an adversary can launch a transfer attack on an MLaaS employing a merged model with over 95% relative transfer ASR.

Next, we define the setup and process under which we statistically evaluate different hypotheses related to how transferability of adversarial examples is influenced by MM. Specifi-

TABLE III ASR matrices $(\{\mathbf{A}_{\gamma}^t\}_{t=1}^T)$ for attack method $\gamma=$ NI-FGSM (in %), showing transferability from surrogate model $s\in\mathcal{S}=\{f_{\boldsymbol{\theta}_0},f_{\boldsymbol{\theta}_t}\}$ to target models $\mathcal{T}.\{\overline{R}_{\gamma}^{t,\,s}\}_{t=1}^T$ is relative mean transfer ASR, denoting success of transfer attack.

Task t	$\mid \mathcal{S} \downarrow / \mathcal{T} \rightarrow$	f_{θ_0}	f_{θ_t}	$f_{\theta_{mtl}^{WA}}$	$f_{m{ heta}_{mtl}^{ ext{TA}}}$	$f_{m{ heta}_{mtl}^{ ext{TM}}}$	$f_{m{ heta}_{mtl}^{ ext{AM}}}$	$f_{\boldsymbol{\theta}_{mtl}^{\text{WA+RS}}}$	$f_{\boldsymbol{\theta}_{mtl}^{\mathrm{TA+RS}}}$	$f_{\boldsymbol{\theta}_{mtl}^{\text{TM+RS}}}$	$f_{\boldsymbol{\theta}_{mtl}^{\text{AM+RS}}}$	$R_{\gamma}^{t, s}$
(t=1) Cars	$\begin{array}{c c} s = f_{\boldsymbol{\theta}_0} \\ s = f_{\boldsymbol{\theta}_t} \end{array}$	87.64 83.61	87.49 97.94	92.22 98.18	82.59 97.14	87.84 97.89	91.05 97.79	91.87 97.91	80.50 96.67	86.89 97.86	89.21 97.64	100.15 99.69
(t=2) MNIST	$\begin{array}{c c} s = f_{\boldsymbol{\theta}_0} \\ s = f_{\boldsymbol{\theta}_t} \end{array}$	94.22 93.24	21.38 99.88	71.98 98.90	44.66 99.30	58.28 99.20	36.50 99.82	70.22 99.40	40.44 99.60	61.32 99.60	38.18 99.82	55.93 99.57
(t=3) EuroSAT	$\begin{array}{c c} s = f_{\boldsymbol{\theta}_0} \\ s = f_{\boldsymbol{\theta}_t} \end{array}$	62.11 56.19	69.15 99.96	79.78 91.70	76.07 90.19	74.37 91.96	70.48 96.11	69.78 98.52	60.56 98.67	62.48 98.89	65.26 98.67	112.46 95.63
(t=4) GTSRB	$\begin{array}{c c} s = f_{\boldsymbol{\theta}_0} \\ s = f_{\boldsymbol{\theta}_t} \end{array}$	80.03 82.66	30.50 99.24	74.76 95.68	59.08 96.14	63.97 96.90	63.71 95.77	65.46 97.10	51.78 96.31	58.27 97.40	58.78 96.47	77.44 97.21
(t=5) SVHN	$\begin{array}{c c} s = f_{\boldsymbol{\theta}_0} \\ s = f_{\boldsymbol{\theta}_t} \end{array}$	89.87 99.35	20.15 98.89	65.09 90.71	55.63 93.97	57.26 94.30	51.83 95.08	59.52 91.75	48.69 94.31	51.62 94.92	54.19 95.90	61.73 94.92
(t=6) RESISC45	$\begin{vmatrix} s = f_{\theta_0} \\ s = f_{\theta_t} \end{vmatrix}$	75.62 71.90	69.84 98.73	79.08 96.00	71.75 95.46	75.17 96.35	75.33 96.63	78.41 96.00	70.38 96.41	72.57 97.68	73.11 97.56	98.49 97.75
(t=7) DTD	$\begin{vmatrix} s = f_{\theta_0} \\ s = f_{\theta_t} \end{vmatrix}$	32.66 22.34	53.94 88.83	71.28 83.83	57.77 82.02	63.83 82.77	64.15 83.09	68.30 86.06	57.13 82.45	61.49 86.38	63.09 85.74	194.06 94.61

 $^{^4}For$ additional context, we include ${\cal S}$ in ${\cal T},$ as it provides information about white-box ASR.

cally, we evaluate three hypotheses: (1) Stronger MM methods increases transferability (\mathcal{H}_1) in §V-A; (2) Mitigating representation bias via RS influences transferability (\mathcal{H}_2) in §V-B; and (3) WA is the most vulnerable to transfer attacks (\mathcal{H}_3) in §V-C. In each of our hypotheses, we are interested in changes/differences in ASR as we go from one condition to another, keeping other conditions the same. For example, in \mathcal{H}_1 , we speculate that the ASR change is positive as we go from a weaker MM method, such as TA, to AM, a relatively stronger MM method, keeping other conditions such as task t, surrogate model s and attack method γ same. Similarly, in \mathcal{H}_2 , we speculate that ASR change is positive/negative as we go from (say) WA to WA+RS, keeping other the conditions same. We identify this as a related design experiment [40]. for which the canonical statistical tests are Student's paired t-test [41] and Wilcoxon signed rank test [42], depending on whether the sample is normal or not. Using this insight, we design a three-step statistical process to evaluate each of our hypothesis:

- 1) **Normality Check.** We first check for normality of the sample, i.e., ASR differences, using Shapiro-Wilk test [43]. Here, the null hypothesis is that the sample is normal, while the alternative is the negation of the null hypothesis.
- Statistical Test. A paired t-test is employed in case the sample is normal, and Wilcoxon's signed rank test otherwise. Specifically,
 - a) if the null hypothesis of normality is not rejected, i.e., $p \geq \alpha$ (where α is the significance level), we perform a one-sample t-test [41] under the null hypothesis: $\mu \leq 0$ versus the one-sided alternative: $\mu > 0$ with significance level α .
 - b) if the normality assumption is rejected $(p < \alpha)$, we instead use the Wilcoxon signed-rank test [42], with the null hypothesis: $\mu_{1/2} \leq 0$ against the one-sided alternative: $\mu_{1/2} > 0$, using the same significance level α , where $\mu_{1/2}$ denotes the median.
- 3) **Benjamini–Hochberg (BH) correction [44].** To correct for multiple comparisons, we apply the BH correction procedure to the obtained p-values, which controls the False Discovery Rate (FDR) Q_e . Here, $Q_e = \mathbb{E}(Q)$, where Q is the proportion of false discoveries among discoveries.

Fig. 2 illustrates this statistical testing procedure. For all tests, we set $\alpha = Q_e = 0.05 = 5 \times 10^{-2}$. Finally, to evaluate the strength of the effect in the hypotheses, we also calculate the effect size for each statistical test performed. For paired t-test, we calculate the effect size d using Cohen's d [45]:

$$d = \frac{\bar{X}_{\mathcal{C}}}{\sigma_{\mathcal{C}}},\tag{14}$$

where $\bar{X}_{\mathcal{C}}$ and $\sigma_{\mathcal{C}}$ are the mean and standard deviation of sample \mathcal{C} consisting of paired differences.

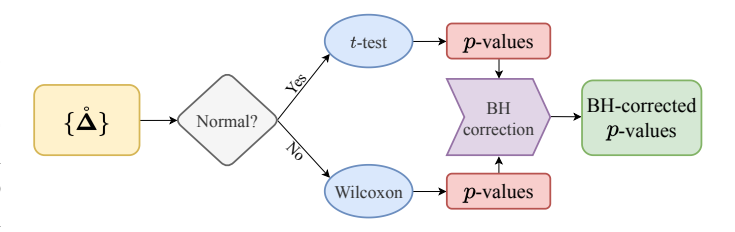


Fig. 2. General statistical testing procedure for investigating transferability in MM. $\{\mathring{\Delta}\}$ denotes set of sets consisting of ASR differences.

For Wilcoxon signed rank test, we calculate the effect size r as follows [46]:

 $r = \frac{Z}{\sqrt{N}},\tag{15}$

where Z is the standardized test statistic from the Wilcoxon test and N is the number of non-zero differences in the sample. A Cohen's d in the range [0.1,0.5), [0.5,0.8), and $[0.8,\infty)$ indicates a small, medium, and large effect respectively [45]. Likewise, a Wilcoxon's r in the range [0.1,0.3), [0.3,0.5), and [0.5,1] indicates a small, medium, and large effect respectively [46]. Values below 0.1 are generally considered negligible.

Note on Confirmatory vs. Exploratory Analysis

Hypothesizing After Results are Known (HARKing) is the questionable practice of creating/changing hypothesis after seeing the patterns in the data and falsely presenting it as an a prior hypothesis [47]. It leads to inflated false positives and problems in reproducibility. We note that most of our hypotheses are confirmatory in nature, i.e., we hypothesized before ever looking at the data/results. However, we found WA to be an outlier while we performed our tests. Therefore, the statistical analysis for \mathcal{H}_3 : WA being the most vulnerable MM method is more exploratory in nature than confirmatory. We also note that the statistical analysis performed in §VII-B for why WA is most vulnerable is confirmatory, i.e., we hypothesized before performing the statistical analysis.

In what follows, Δ denotes the difference in ASR between two conditions, Δ denotes the tensor collecting these ASR differences, and $\mathring{\Delta}$ denotes a set having entries of Δ as its elements. Formally, $\mathring{\Delta} := \left\{ \Delta_{i_1,i_2,\dots,i_q} \mid (i_1,i_2,\dots,i_q) \in \mathcal{I} \right\}$ where q is the rank of the tensor (i.e., the number of dimensions), $\mathcal{I} = [n_1] \times \dots \times [n_q]$ is the $index\ space,\ \Delta_{i_1,\dots,i_q}$ denotes the $scalar\ entry\ (i_1,\dots,i_q)$ of the tensor Δ .

A. Stronger Merging Increases Transferability

Hypothesis \mathcal{H}_1 . Employing a stronger MM method results in a higher transfer ASR.

In particular, we test whether ASR increases when moving from TA or TM to AM. We do not compare TA and TM

since we find no significant difference in their performance (cf. TABLE II).

Setup. To test \mathcal{H}_1 , we extract paired differences in ASR between AM and two baseline merging methods (TA and TM), both with and without RS. Specifically, for each $\gamma \in \Gamma$, task $t \in [T]$ and surrogate $s \in \mathcal{S} = \{f_{\theta_0}, f_{\theta_t}\}$, we compute:

$$\Delta_{\mathrm{AM, TA}}^{(s,t,\gamma)} = [\mathbf{A}_{\gamma}^t]_{s,\,f_{\boldsymbol{\theta}_{mtl}^{\mathrm{AM}}}} - [\mathbf{A}_{\gamma}^t]_{s,\,f_{\boldsymbol{\theta}_{mtl}^{\mathrm{TA}}}}, \tag{16}$$

$$\Delta_{\mathrm{AM,\,TM}}^{(s,t,\gamma)} = [\mathbf{A}_{\gamma}^t]_{s,\,f_{\boldsymbol{\theta}_{mtl}^{\mathrm{AM}}}} - [\mathbf{A}_{\gamma}^t]_{s,\,f_{\boldsymbol{\theta}_{mtl}^{\mathrm{TM}}}}, \tag{17}$$

and collect them into tensors:

$$\Delta_{\text{AM, TA}} \in [0, 1]^{|\mathcal{S}| \times T \times |\Gamma|},$$
 (18)

$$\Delta_{\text{AM, TM}} \in [0, 1]^{|\mathcal{S}| \times T \times |\Gamma|}.$$
 (19)

Similarly, for its RS-variants, we compute:

$$\Delta_{\text{AM+RS, TA+RS}}^{(s,t,\gamma)} = [\mathbf{A}_{\gamma}^t]_{s,\,f_{\boldsymbol{\theta}_{mtl}^{\text{AM+RS}}}} - [\mathbf{A}_{\gamma}^t]_{s,\,f_{\boldsymbol{\theta}_{mtl}^{\text{TA+RS}}}}, \tag{20}$$

$$\Delta_{\text{AM+RS, TM+RS}}^{(s,t,\gamma)} = [\mathbf{A}_{\gamma}^t]_{s, f_{\boldsymbol{\theta}_{mtl}^{\text{AM+RS}}}} - [\mathbf{A}_{\gamma}^t]_{s, f_{\boldsymbol{\theta}_{mtl}^{\text{TM+RS}}}}. \tag{21}$$

and collect them into tensors:

$$\boldsymbol{\Delta}_{\text{AM+RS, TA+RS}}^{\gamma} \in [0,1]^{|\mathcal{S}| \times T} \; \forall \; \gamma \in \Gamma, \tag{22}$$

$$\Delta_{\text{AM+RS, TA+RS}} \in [0, 1]^{|\mathcal{S}| \times T \times |\Gamma|},$$
 (23)

$$\Delta_{\text{AM+RS, TM+RS}}^{\gamma} \in [0, 1]^{|\mathcal{S}| \times T} \ \forall \ \gamma \in \Gamma,$$
 (24)

$$\Delta_{\text{AM+RS, TM+RS}} \in [0, 1]^{|\mathcal{S}| \times T \times |\Gamma|}.$$
 (25)

Statistical **Testing** Results. We perform statistical the four difference sample sets tests for each of $(\Delta_{AM, TA}, \Delta_{AM, TM}, \Delta_{AM+RS, TA+RS}, \Delta_{AM+RS, TM+RS})$ attack-specific difference with sample $\operatorname{sets}\left(\mathring{\boldsymbol{\Delta}}_{\operatorname{AM, TA}}^{\gamma}, \mathring{\boldsymbol{\Delta}}_{\operatorname{AM, TM}}^{\gamma}, \mathring{\boldsymbol{\Delta}}_{\operatorname{AM+RS, TA+RS}}^{\gamma}, \mathring{\boldsymbol{\Delta}}_{\operatorname{AM+RS, TM+RS}}^{\gamma} \ \forall \ \gamma \ \in$ Γ), while applying BH correction separately to the two groups: with and without RS. For brevity, we defer the results for attack-specific differences to Appendix D. TABLE IV and TABLE V report the results of the statistical tests performed on two main groups, while Fig. 3 and Fig. 4 visualize them. In both TABLE IV and TABLE V, we see a statistically significant difference for all of the sample sets we perform the

test on. Moreover, in both the groups (with and without RS), we find the effect size for TA to be large, while the effect size for TM to be small. These observations suggest that AM is a significantly more vulnerable method than TA, while being only slightly more vulnerable than TM. This is also evident from the distributions in Fig. 3 and Fig. 4, which visualize $\mathring{\Delta}_{AM, TA}, \mathring{\Delta}_{AM, TM}$ and $\mathring{\Delta}_{AM+RS, TA+RS}, \mathring{\Delta}_{AM+RS, TM+RS},$ respectively.

Takeaway

Employing a stronger MM method such as AM, in expectation of performance gains, would inadvertently also increase the threat of transfer attack to a large extent. Specifically, we observe statistical significance for all tests, with large effect size when comparing TA to AM, while only small effect size when comparing TM to AM. Therefore, AM is significantly more vulnerable than TA, while only being marginally more vulnerable than TM.

We further discuss the reason for this finding in §VII-A.

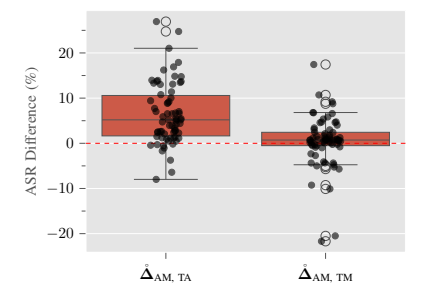


Fig. 3. Box-jitter plot of $\mathring{\Delta}_{AM, TA}$ and $\mathring{\Delta}_{AM, TM}$.

B. Mitigating Representation Bias Influences Transferability

We divide hypothesis \mathcal{H}_2 into two sub-hypothesis:

TABLE IV STATISTICAL TEST RESULTS FOR \mathcal{H}_1 : STRONGER MERGING INCREASES TRANSFERABILITY (WITHOUT RS).

Sample	Shapiro–Wilk p -value	Normal?	Test Used	Test Statistic	One-tailed p -value	BH-corrected p -value	Effect Size
$\mathring{\Delta}_{\mathrm{AM,TA}}$ $\mathring{\Delta}_{\mathrm{AM,TM}}$	1.22×10^{-2} 1.09×10^{-6}	No No		W = 2338.0 W = 1597.5	7.22×10^{-11} 1.89×10^{-2}	1.44×10^{-10} 1.89×10^{-2}	r = 0.766 r = 0.248

TABLE V STATISTICAL TEST RESULTS FOR \mathcal{H}_1 : STRONGER MERGING INCREASES TRANSFERABILITY (WITH RS).

Sample	Shapiro-Wilk p -value	Normal?	Test Used	Test Statistic	One-tailed p -value	BH-corrected p-value	Effect Size
$\mathring{\Delta}_{AM+RS, TA+RS}$	1.90×10^{-3}	No	Wilcoxon	W = 2410.0	4.17×10^{-12}	8.35×10^{-12}	r = 0.817
$\mathring{\Delta}_{AM+RS, TM+RS}$	2.60×10^{-9}	No	Wilcoxon	W = 1635.0	1.08×10^{-2}	1.08×10^{-2}	r = 0.275

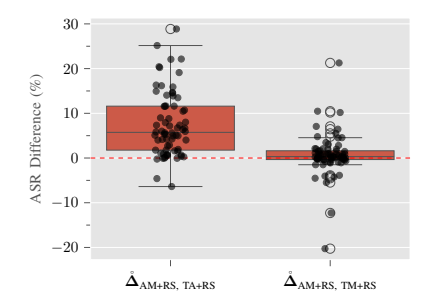


Fig. 4. Box-jitter plot of $\mathring{\Delta}_{AM+RS, TA+RS}$ and $\mathring{\Delta}_{AM+RS, TM+RS}$.

- 1) **Hypothesis** \mathcal{H}_{2a} . When using pretrained model as surrogate, reducing representation bias via RS leads to a decrease in transfer ASR.
- 2) **Hypothesis** \mathcal{H}_{2b} . When using fine-tuned model as surrogate, reducing representation bias via RS leads to an increase in transfer ASR.

Setup. To test \mathcal{H}_{2a} , for each merging method $m_{\text{base}} \in \mathcal{M}_{\text{base}} = \{\text{WA}, \text{TA}, \text{TM}, \text{AM}\}$, we consider its RS-augmented counterpart $m_{\text{RS}} = m_{\text{base}} + \text{RS}$. For each task $t \in [T]$ and each attack method $\gamma \in \Gamma$, we compute the difference in ASR between the base model and its corresponding RS variant, under a fixed surrogate model. Specifically, when the surrogate model is a PTM f_{θ_0} , we define the difference:

$$\Delta_{m_{\text{base}}}^{(t,\gamma)} = [\mathbf{A}_{\gamma}^t]_{f_{\boldsymbol{\theta}_0}, f_{\boldsymbol{\theta}_{mt}^{m_{\text{base}}}}} - [\mathbf{A}_{\gamma}^t]_{f_{\boldsymbol{\theta}_0}, f_{\boldsymbol{\theta}_{mt}^{m_{\text{RS}}}}}, \tag{26}$$

for each $m_{\text{base}} \in \mathcal{M}_{\text{base}}$.

This results in $|\mathcal{M}_{\text{base}}|$ ASR differences per task, per attack method. We collect these differences across T tasks to obtain the difference tensor:

$$\Delta_{\text{PTM}}^{\gamma} \in [0, 1]^{|\mathcal{M}_{\text{base}}| \times T}, \quad \forall \gamma \in \Gamma.$$
(27)

We also collect all $|\Gamma|$ difference tensors $(\{\Delta_{\text{PTM}}^{\gamma} | \gamma \in \Gamma\})$ into a single tensor to form:

$$\Delta_{\text{PTM}}^{\text{all}} \in [0, 1]^{|\mathcal{M}_{\text{base}}| \times T \times |\Gamma|}.$$
 (28)

To test hypothesis \mathcal{H}_{2a} , the above procedure is repeated for the case where the surrogate model is a fine-tuned model f_{θ_t} , except now, we define the difference as:

$$\Delta_{m_{\text{base}}}^{(t,\gamma)} = [\mathbf{A}_{\gamma}^t]_{f_{\boldsymbol{\theta}_t}, f_{\boldsymbol{\theta}_{mtl}^{m_{\text{RS}}}}} - [\mathbf{A}_{\gamma}^t]_{f_{\boldsymbol{\theta}_t}, f_{\boldsymbol{\theta}_{mtl}^{m_{\text{base}}}}}, \tag{29}$$

resulting in analogous difference tensors:

$$\Delta_{\text{FT}}^{\gamma} \in [0, 1]^{|\mathcal{M}_{\text{base}}| \times T}, \quad \Delta_{\text{FT}}^{\text{all}} \in [0, 1]^{|\mathcal{M}_{\text{base}}| \times T \times |\Gamma|}.$$
 (30)

Statistical Testing Results. We perform statistical tests on each of $2(|\Gamma|+1)$ difference sample sets (viz., $\{\mathring{\Delta}_{PTM}^{\gamma} \mid \gamma \in \Gamma\}$, $\mathring{\Delta}_{PTM}^{all}$, $\{\mathring{\Delta}_{PTM}^{\gamma} \mid \gamma \in \Gamma\}$, $\mathring{\Delta}_{FT}^{all}$). TABLE VI and TABLE VII report the results for \mathcal{H}_{2a} and \mathcal{H}_{2b} , respectively. From TABLE VI, we see a statistically significant difference for all of samples we perform the statistical test on. Moreover, we see a large effect size for all the tests. This suggests mitigating representation bias decreases vulnerability to transfer attacks to a large extent, if the surrogate model is a PTM. This is also evident from the distribution of $\{\mathring{\Delta}_{PTM}^{\gamma} \mid \gamma \in \Gamma\}$ and $\mathring{\Delta}_{PTM}^{all}$ as shown in Fig. 5 and Fig. 6, respectively. Therefore, from \mathcal{A} 's perspective which only has access to the commonly available pre-trained checkpoint of the model f_{θ_0} , RS lowers the chance of launching a successful transfer attack and is consequently

TABLE VI Statistical test results for \mathcal{H}_{2a} : transferability decreases upon bias mitigation when the surrogate is a PTM.

Sample	Shapiro-Wilk p-value	Normal?	Test Used	Test Statistic	One-tailed p-value	BH-corrected p-value	Effect Size
$\mathring{\Delta}_{\mathrm{PTM}}^{\mathrm{FGSM}}$	4.64×10^{-1}	Yes	t-test	$t_s = 5.55$	3.46×10^{-6}	4.33×10^{-6}	d = 1.484
$\mathring{\Delta}_{\mathrm{PTM}}^{\mathrm{I-FGSM}}$	1.08×10^{-1}	Yes	t-test	$t_s = 6.43$	3.43×10^{-7}	5.72×10^{-7}	d=1.718
$\mathring{\Delta}_{\mathrm{PTM}}^{\mathrm{PGD}}$	1.20×10^{-2}	No	Wilcoxon	W = 405.0	7.45×10^{-9}	4.36×10^{-5}	r = 0.869
$\mathring{\Delta}_{\mathrm{PTM}}^{\mathrm{NI-FGSM}}$	4.19×10^{-2}	No	Wilcoxon	W = 32.5	1.19×10^{-5}	1.19×10^{-5}	r = 0.734
$\mathring{\Delta}_{\mathrm{PTM}}^{\mathrm{TI-FGSM}}$	9.71×10^{-3}	No	Wilcoxon	W = 11.0	2.05×10^{-7}	5.13×10^{-7}	r = 0.826
$\mathring{f\Delta}^{ m all}_{ m PTM}$	5.80×10^{-4}	No	Wilcoxon	W=295.5	4.12×10^{-17}	2.06×10^{-16}	r = 0.805

TABLE VII

Statistical test results for \mathcal{H}_{2b} : transferability increases upon bias mitigation when the surrogate is a fine-tuned model. $p ext{-values} > \alpha = 0.05$ are underlined (red).

Sample	Shapiro-Wilk p-value	Normal?	Test Used	Test Statistic	One-tailed p-value	BH-corrected p-value	Effect Size
$\mathring{\Delta}_{\mathrm{FT}}^{\mathrm{FGSM}}$	5.20×10^{-4}	No	Wilcoxon	W = 105.0	9.88×10^{-1}	9.88×10^{-1}	r = -0.421
$\mathring{\Delta}_{\mathrm{FT}}^{\mathrm{I-FGSM}}$	2.03×10^{-1}	Yes	t-test	$t_s = 2.46$	1.04×10^{-2}	1.45×10^{-2}	d = 0.656
$\mathring{\Delta}_{\mathrm{FT}}^{\mathrm{PGD}}$	1.23×10^{-2}	No	Wilcoxon	W = 375.0	8.83×10^{-6}	3.09×10^{-5}	r = 0.740
$\mathring{\Delta}_{\mathrm{FT}}^{\mathrm{NI-FGSM}}$	1.00×10^{-5}	No	Wilcoxon	W = 15.0	1.45×10^{-5}	3.39×10^{-5}	r = 0.805
$\mathbf{\Delta}_{\mathrm{FT}}^{\mathrm{TI-FGSM}}$	4.65×10^{-2}	No	Wilcoxon	W = 137.0	$\underline{6.88\times10^{-2}}$	$\underline{8.02\times10^{-2}}$	r = 0.284
$\mathring{\Delta}_{\mathrm{FT}}^{\mathrm{all}}$	2.44×10^{-9}	No	Wilcoxon	W=6772.0	3.04×10^{-5}	5.33×10^{-5}	r = 0.340
$\mathring{\Delta}_{\mathrm{FT}}^{\mathrm{sig}}$	6.13×10^{-6}	No	Wilcoxon	W=3067.0	9.21×10^{-10}	6.44×10^{-9}	r = 0.660

undesirable. Likewise, from \mathcal{O} 's perspective, RS not only leads to significant accuracy gains, but also leads to an unintentional defense against weak (f_{θ_0} -equipped) attacks. However, the results from statistical test performed for \mathcal{H}_{2b} reveal a different narrative. In TABLE VII, we observe the test to be statistically significant for $\mathring{\Delta}_{FT}^{\gamma} \forall \gamma \in \{\text{I-FGSM, PGD, NI-FGSM}\}$ and borderline significant for $\mathring{\Delta}_{FT}^{TI\text{-FGSM}}$. Moreover, we find the effect size to be large for $\mathring{\Delta}_{FT}^{\gamma} \forall \gamma \in \{PGD, NI\text{-}FGSM\},$ moderate for $\mathring{\Delta}_{FT}^{I\text{-}FGSM}$ and small for $\mathring{\Delta}_{FT}^{TI\text{-}FGSM}$. This suggests that mitigating bias using RS inadvertently raises the threat of transfer attack significantly when surrogate is a fine-tuned model $f_{\theta_{+}}$, evident from the distribution shown in Fig. 7. This is desirable to a stronger A that employs f_{θ_t} as the surrogate, while being undesirable to \mathcal{O} . Finally, we do not observe statistical significance for $\mathring{\Delta}_{FT}^{FGSM}$. In fact, we find a moderate effect in the opposite direction, upon inspecting the effect size r = -0.421 in TABLE VII and distribution of $\mathring{\Delta}_{\mathrm{FT}}^{\mathrm{FGSM}}$ in Fig. 7. This means an O using RS would be defended against an A employing FGSM as her attack. This might seem contradictory to \mathcal{H}_{2b} at first. However, this is expected, since we previously established from \mathcal{H}_{2a} that using RS helps defend against weak attacks. FGSM is a single-step attack, and the weakest attack when compared against other iterative attacks in our work (cf. TABLE E.1). The small effect size for TI-FGSM can similarly be explained by observing lower ASR relative to other methods (cf. TABLES E.2 E.3 E.4) To further validate this, we isolate the effect of the statistically significant results, and collect $\Delta_{\mathrm{FT}}^{\gamma} \, \forall \, \gamma \in \Gamma \backslash \{\mathrm{FGSM}, \, \mathrm{TI-FGSM}\}$ into tensor Δ_{FT}^{sig} and test for sample set $\mathring{\Delta}_{FT}^{sig} = \mathring{\Delta}_{FT}^{all} \backslash \{\mathring{\Delta}_{FT}^{FGSM} \cup \mathring{\Delta}_{FT}^{TI-FGSM}\}$. We find a statistically significant result for $\mathring{\Delta}_{FT}^{sig}$ with large effect size as seen in TABLE VII and its distribution in Fig. 8, corroborating hypothesis \mathcal{H}_{2b} .

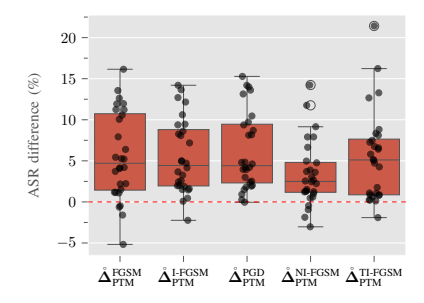


Fig. 5. Box-jitter plot of $\mathring{\mathbf{\Delta}}_{PTM}^{\gamma} \, \forall \, \gamma \in \Gamma$.

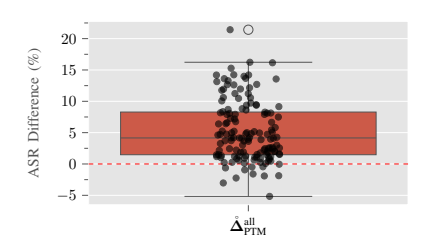


Fig. 6. Box-jitter plot of $\mathring{\Delta}_{PTM}^{all}$.

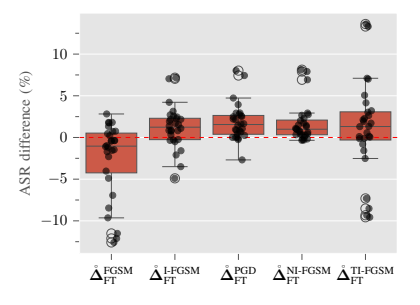


Fig. 7. Box-jitter plot of $\mathring{\Delta}_{FT}^{\gamma} \forall \gamma \in \Gamma$.

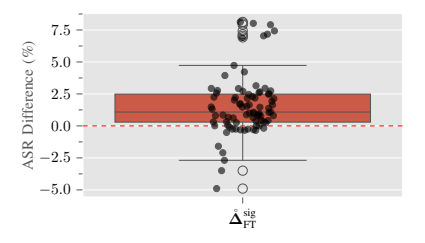


Fig. 8. Box-jitter plot of $\mathring{\Delta}_{FT}^{sig} = \mathring{\Delta}_{FT}^{all} \setminus \{\mathring{\Delta}_{FT}^{FGSM} \cup \mathring{\Delta}_{FT}^{TI-FGSM}\}.$

Takeaway

Mitigating representation bias can only defend against weaker attacks (e.g., attacks employing a weaker surrogate f_{θ_0} , or employing a weaker attack method, such as FGSM). In the face of a strong attack (e.g., attacks employing a stronger surrogate f_{θ_t} or a strong attack method, such as PGD or NI-FGSM), the threat of transfer attack increases significantly for owner. Indeed, there is no such thing as a "free lunch".

We further discuss the reason for this finding in §VII-A.

C. Weight Averaging is Most Vulnerable to Transfer Attacks

Hypothesis \mathcal{H}_3 . WA yields the highest transfer ASR despite being the weakest MM method.

Setup. For each task $t \in [T]$, surrogate model $s \in \mathcal{S} = \{f_{\theta_0}, f_{\theta_t}\}$, and attack method $\gamma \in \Gamma$, we compare WA against the other base merging methods: TA, TM, and AM. We define the difference in ASR between WA and another merging method $m \in \{\text{TA}, \text{TM}, \text{AM}\} = \mathcal{M}_{\text{WA}'}$ for task t and surrogate s as:

$$\Delta_{\text{WA}, m}^{(s,t,\gamma)} = [\mathbf{A}_{\gamma}^t]_{s, f_{\boldsymbol{\theta}_{mtl}^{\text{WA}}}} - [\mathbf{A}_{\gamma}^t]_{s, f_{\boldsymbol{\theta}_{mtl}^m}}.$$
 (31)

We compute $\Delta_{\mathrm{WA},m}^{(s,t,\gamma)}$ for both $s \in \mathcal{S}$ and for each $t \in [T]$, resulting in $|\mathcal{S}|$ values per task. Collecting these differences across T tasks yields the difference tensor:

$$\Delta_{\text{WA}, m}^{\gamma} \in [0, 1]^{|\mathcal{S}| \times T}, \forall m \in \mathcal{M}_{\text{WA}'}.$$
 (32)

Finally, we collect all difference tensors $|\Gamma|$ $\{\Delta_{\mathrm{WA},m}^{\gamma}\,|\,\gamma\in\Gamma\}$ to form the tensor:

$$\Delta_{\text{WA},m} \in [0,1]^{|\mathcal{S}| \times T \times |\Gamma|}.$$
 (33)

TABLE VIII STATISTICAL TEST RESULTS FOR \mathcal{H}_3 (WITHOUT RS): WA IS MORE VULNERABLE THAN TA, TM, AM.

Sample	Shapiro-Wilk p-value	Normal?	Test Used	Test Statistic	One-tailed p -value	BH-corrected p-value	Effect Size
$\overset{\circ}{\mathbf{\Delta}}_{\mathrm{WA, TA}}$ $\overset{\circ}{\mathbf{\Delta}}_{\mathrm{WA, TM}}$ $\overset{\circ}{\mathbf{\Delta}}_{\mathrm{WA, AM}}$	4.36×10^{-2} 8.12×10^{-3} 2.80×10^{-4}	No No No	Wilcoxon Wilcoxon Wilcoxon	W = 1563.0 W = 1473.0 W = 1215.0	2.19×10^{-10} 1.84×10^{-8} 3.35×10^{-4}	6.57×10^{-10} 2.76×10^{-8} 3.35×10^{-4}	r = 0.810 r = 0.710 r = 0.444

TABLE IX STATISTICAL TEST RESULTS FOR \mathcal{H}_3 (with RS): WA+RS is more vulnerable than TA+RS, TM+RS, AM+RS.

Sample	Shapiro-Wilk p-value	Normal?	Test Used	Test Statistic	One-tailed p-value	BH-corrected p-value	Effect Size
$\mathring{\Delta}$ WA+RS, TA+RS $\mathring{\Delta}$ WA+RS, TM+RS $\mathring{\Delta}$ WA+RS, AM+RS	6.95×10^{-3} 2.25×10^{-2} 3.00×10^{-6}	No No No	Wilcoxon Wilcoxon Wilcoxon	W = 1557.0 W = 1478.0 W = 1281.5	2.98×10^{-10} 1.45×10^{-8} 9.00×10^{-6}	8.94×10^{-10} 2.18×10^{-8} 9.00×10^{-6}	r = 0.821 r = 0.740 r = 0.585

We repeat this process independently for RS-augmented variants. For the RS variants, the difference is defined as:

$$\Delta_{\text{WA+RS}, m+\text{RS}}^{(s,t,\gamma)} = [\mathbf{A}_{\gamma}^t]_{s, f_{\boldsymbol{\theta}_{mtl}^{\text{WA+RS}}}} - [\mathbf{A}_{\gamma}^t]_{s, f_{\boldsymbol{\theta}_{mtl}^{m+\text{RS}}}}, \tag{34}$$

with corresponding difference tensors:

$$\Delta_{\text{WA+RS}, m+\text{RS}}^{\gamma} \in [0, 1]^{|\mathcal{S}| \times T}, \forall m \in \mathcal{M}_{\text{WA}'}.$$
 (35)

$$\Delta_{\text{WA+RS}, m+\text{RS}} \in [0, 1]^{|\mathcal{S}| \times T \times |\Gamma|}, \forall m \in \mathcal{M}_{\text{WA}'}.$$
 (36)

Statistical Testing Result. We perform statistical tests for $\mathring{\Delta}_{WA,\,m}^{\gamma}$, $\mathring{\Delta}_{WA+RS,\,m+RS}^{\gamma}$, $\mathring{\Delta}_{WA,\,m}^{\gamma}$, $\mathring{\Delta}_{WA+RS,\,m+RS}^{\gamma}$, $\mathring{\Delta}_{WA,\,m}^{\gamma}$, $\mathring{\Delta}_{WA+RS,\,m+RS}^{\gamma}$, $\mathring{\Delta}_{WA+RS,\,m+RS}^{\gamma}$, $\mathring{\Delta}_{WA+RS,\,m+RS}^{\gamma}$, and apply BH correction to each of the groups (with and without RS) separately. For brevity, we defer results of attack-specific samples to Appendix D. TABLE VIII and TABLE IX show the results for $\mathring{\Delta}_{WA,\,m}^{\gamma}$ and $\mathring{\Delta}_{WA+RS,\,m+RS}^{\gamma}$, $\forall\,m\in\mathcal{M}_{WA'}^{\gamma}$, respectively. We find statistically significant results for all sample sets we perform the test on. Moreover, we find a large effect size for all samples except $\mathring{\Delta}_{WA,\,AM}^{\gamma}$ where the effect size is medium. This means WA increases the threat of transfer attack significantly, which can be verified from the distributions given in Fig. 9 and Fig. 10.

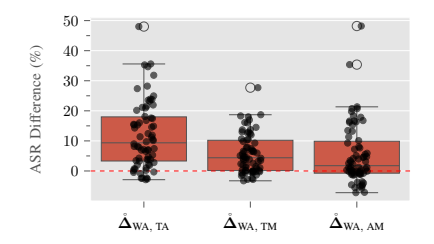


Fig. 9. Box-jitter plot of $\mathring{\Delta}_{WA, m} \forall m \in \mathcal{M}_{WA'}$.

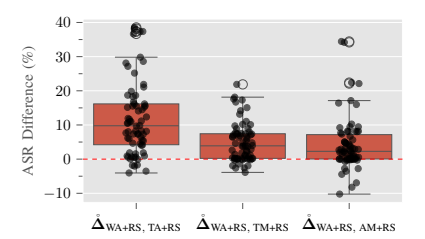


Fig. 10. Box-jitter plot of $\mathring{\Delta}_{WA+RS, m+RS} \forall m \in \mathcal{M}_{WA'}$.

Takeaway

Despite being the weakest MM method, WA increases the threat of transfer attack the most. Consequently, an owner suffers not only from poor multi-task model performance when employing WA, but also increases her threat to transfer attacks the most.

We further discuss the reason for this finding in §VII-B.

VI. RELATED WORKS

Early works [48], [49], [50], [51] demonstrate that when two neural networks share part of their optimization trajectory, their weights can often be linearly interpolated without degrading performance—a phenomenon known as *Linear* Mode Connectivity (LMC). Subsequent studies extend this to feature space, introducing Layerwise Linear Feature Connectivity (LLFC), where the interpolated model features are proportional to those of its endpoints [52]. More recently, Zhou et al. [53] show that LLFC holds in the pretraining-finetuning paradigm, and identify a stronger notion of linearity than LLFC, termed Cross Task Linearity (CTL), which asserts the features in the weight-interpolated model are approximately equal to the linear interpolation of features in the two finetuned models at each layer. In doing so, they provide explanation for why MM methods such as WA and TA work. These findings offer a new perspective on MM, which has been employed for enhancing generalization [7], [54], [55], [56], constructing multi-task models [8], [9], [10], [11], and supporting domains like parameter-efficient tuning [57], [58], reinforcement learning [59], and diffusion models [60], [61].

Despite its broad applicability, the security implications of MM has largely remained unexplored, with only few works recently examining it. Arora et al. [13] are first to observe MM mitigates backdoors. Specifically, by merging a poisoned model with a clean counterpart using WA, the merged model maintains high clean accuracy while significantly reducing backdoor ASR, thereby giving a "free lunch" of adversarial robustness. Concurrently, BadMerging [62] proposed by Zhang et al., also notes vanilla MM mitigates backdoor attacks, and designs persistent backdoors in the individual fine-tuned models that survive merging process by crafting a universal trigger. With this, BadMerging achieves up to 95% ASR in the merged model. More recently, Wang et al. [63] introduce MergeBackdoor, a novel supply-chain threat for MM in which seemingly benign models when merged result in backdoored model. Concurrently, Yuan et al. [64] introduce Merge Hijacking, the first backdoor attack against MM in large language models. In all these works, vanilla MM pipeline is assumed to be harmless, with adversary disrupting the MM pipeline for attack. In contrast, our work highlights vulnerabilities inherent to MM, i.e., without ever disrupting the MM pipeline, we show how MM is not just susceptible, but increases the threat to transfer attacks.

The most related work to our is by Gangwal and Sharma [65], which investigates transferability of adversarial examples in MM. However, their preliminary analysis consists of only two MM methods and three datasets, and does not consist of rigorous statistical evaluations as ours. Moreover, it alludes to MM providing "free" adversarial robustness, similar to Arora et al., which is the notion we challenge. Our work is, to our best knowledge, the first to systematically and extensively study the risk of transfer attacks in the context of MM methods, and show that MM increases the threat to transferable adversarial examples, along with providing other key insights.

VII. DISCUSSION

A. Stronger Merging Methods, Representation Surgery and **Transferability**

Explaining Higher Transferability for Stronger Merging Methods (\mathcal{H}_1). In §V-A, we observe stronger MM methods tend to have higher transferability. Prior works have shown decision boundary similarity [20], [21] and higher accuracy of target model [17] are correlated with higher transferability. Since the goal of MM is minimizing the loss on the test set across multiple tasks (cf. Eq. (1)), it explains higher transferability of stronger MM methods.

Explaining the Effect of Representation Bias in Trans**ferability** (\mathcal{H}_{2a} and \mathcal{H}_{2b}). In §V-B, we observe that when the surrogate is a PTM, reducing representation bias leads to lower transferability (\mathcal{H}_{2a}) , while when the surrogate is a fine-tuned model, reducing representation bias leads to higher transferability (\mathcal{H}_{2b}) . To explain this, we observe that minimizing the objective in Eq. (7) pulls representations obtained from the merged model $(\widehat{\boldsymbol{Z}}_{mtl}^t)$ closer to representations obtained from the individual, fine-tuned models (Z_{ind}^t). Since during classification, the classifier head for every task is reused in the merged model, it means reducing representation bias is the same as making the merged model's decision boundary closer to the fine-tuned models. This explains \mathcal{H}_{2b} , since now the target (RS-augmented) model's decision boundary aligns more surrogate (fine-tuned) model than its RS-free counterpart. It also explains \mathcal{H}_{2a} , since it simultaneously makes the target (RS-augmented) model's decision boundary dissimilar to PTM's.

B. Weight Averaging and Transferability

Explaining Higher Transferability of Weight Averaging (\mathcal{H}_3) . In §V-C, we observe WA consistently exhibits higher transferability than all other MM methods, despite being the weakest merging method in terms of test accuracy [11]. To understand this, we look at CTL [53], which shows that for each layer ℓ and input x,

$$f_{\boldsymbol{\theta}_{mtl}^{\text{WA}}}^{(\ell)}(\mathbf{x}) = f_{\frac{1}{T}\sum_{t}\boldsymbol{\theta}_{t}}^{(\ell)}(\mathbf{x}) \approx \frac{1}{T}\sum_{t=1}^{T}f_{\boldsymbol{\theta}_{t}}^{(\ell)}(\mathbf{x}).$$
(37)

If we set $\ell = L$ (the last layer) in Eq. (37), we find the prediction of WA approximates the logit ensemble of individual models. We conjecture this enables WA model's gradient to be approximately at the center of individual models' gradient directions. Mathematically,

$$\nabla_{\mathbf{x}} \mathcal{L} \left(f_{\boldsymbol{\theta}_{mtl}^{\text{WA}}}(\mathbf{x}), \mathbf{y} \right) \approx \frac{1}{T} \sum_{t=1}^{T} \frac{\nabla_{\mathbf{x}} \mathcal{L} \left(f_{\boldsymbol{\theta}_{t}}(\mathbf{x}), \mathbf{y} \right)}{|\nabla_{\mathbf{x}} \mathcal{L} \left(f_{\boldsymbol{\theta}_{t}}(\mathbf{x}), \mathbf{y} \right)|}.$$
(38)

Consequently, this maximizes the average cosine similarity between surrogate and target model's gradient (cf. Appendix C for proof), and leads to high alignment between them, which is a well-known driver for transferability [17], [18], [66]. This makes WA more susceptible to adversarial transfer than other MM methods that move the target model's gradient direction away from the center with scaling coefficient $\lambda \neq 1/T$.

We test this conjecture by checking whether a merged model's input gradient points to the empirical center of the individual gradient directions. For a sample (\mathbf{x}, \mathbf{y}) let $g_t = \nabla_{\mathbf{x}} \mathcal{L} \left(f_{\boldsymbol{\theta}_t}(\mathbf{x}), \mathbf{y} \right), \ \hat{g}_t = \frac{g_t}{\|g_t\|}, \ \bar{g} = \frac{1}{T} \sum_{t=1}^T \hat{g}_t, \ \hat{\bar{g}} = \bar{g}/\|\bar{g}\|.$ Then for a merged model M with unit gradient \hat{g}_M , define

the center score c

$$c(M) = \langle \hat{g}_M, \hat{\bar{g}} \rangle. \tag{39}$$

We find the mean c to be 0.0283 and 0.0087 for WA and other methods, respectively, indicating WA's gradient are positioned relatively closer towards center of individual models' unit gradient than other methods. We perform a Mann-Whitney U test [67] to confirm the statistical significance and find p-value to be 1.832×10^{-6} , indicating the difference is non-trivial. Finally, we also calculate the alignment between the gradients of surrogate and target models for each method with mean cosine similarity between them. We find the score for WA and other methods to be 0.0827 and 0.0089, respectively with a Mann-Whitney p-value 8.131×10^{-47} , indicating surrogate model's gradients do indeed align better with WA than other methods, making WA naturally more susceptible to transfer attacks than other methods.

C. Targeted Attacks

Throughout the paper, we have assumed the attacks to be untargeted. However, an adversary may have incentive to perform targeted attacks. Therefore, we perform targeted attacks using $\gamma=\text{NI-FGSM}\ \forall$ target models and datasets. Appendix F presents the result of attack performed. When considering pretrained model as surrogate, we find the average $\overline{R}_{\gamma}^{t,\,s}$ to only 0.14%. This indicates MM is able to successfully defend against targeted attacks performed using pretrained models as surrogate. However, we also find $\overline{R}_{\gamma}^{t,\,s}=80.55\%$ when the surrogate is fine-tuned model, indicating MM cannot defend against targeted attacks performed using fine-tuned models as the surrogate.

D. Query-based (black-box) Attacks

Although our work focuses primarily on the black-box setting of transferability of adversarial examples in model merging, we find it imperative to test the MM methods against another class of black-box attacks: query-based attacks. We employ the Square Attack [27] to attack the merged models. We presents the results of attack performed in Appendix H. Here, we find the ASR is no less than 80% for 43/56 cases, with average ASR = 85.00%, indicating MM cannot reliably defend against query-based black-box attacks as well.

E. Attack with Different Surrogate

So far, we have assumed adversary to know owner uses a merged model, the architecture of the merged model, and having access to the corresponding pretrained/fine-tuned model. However, even if pretrained/fine-tuned models of the corresponding architecture are readily available, knowing the architecture may not always be feasible. Therefore, we test whether MM can defend against attacks performed with surrogate having different architecture. Specifically, we present the result on CLIP models with ResNet-50 backbone in Appendix VII-E. Here, we observe that when surrogate is pretrained, average $\overline{R}_{\gamma}^{t,s}$ of 88.97%. However, this average is skewed due to few relatively high values of $\overline{R}_{\gamma}^{t,\,s},$ with the median being 57.73%. This means when using pretrained as a surrogate. MM is successfully able to defend sometimes. while in others, it even amplifies the effect of the attack. When surrogate is fine-tuned, we find average $\overline{R}_{\gamma}^{t,s}$ as 114%and median as 103.66%. This means attacks performed on MM using different architecture (e.g., ResNet-50) could be even more effective than its white-box counterpart. Overall, we find even with a different surrogate, MM cannot reliably defend against transfer attacks.

F. Towards Mitigation and Robust Model Merging

MM offers multi-task capability without joint training or access to all task data, making it a cost-effective alternative to multi-task learning (MTL). However, there are no works

analyzing transferability of adversarial examples (and defense) in the context of MTL. There are few works that address white-box adversarial robustness in MTL [21], [68], [69], [70]. However, they are not directly applicable, as MTL models can be made adversarially robust during training (i.e., adversarial training), whereas merged models cannot, since there is no training phase after merging due to lack of access to taskspecific training dataset. Therefore, we test the efficacy of common input transformation defenses against adversarial examples. We test three input transformation defenses from Guo et al. [71]: (1) Crop Ensemble, i.e., cropping and rescaling images and averaging prediction over multiple crops; (2) Bitdepth Reduction; and (3) JPEG Compression. We also test SND [72] (adding small Gaussian noise to input), an input transformation defense against query-based attacks due to its simplicity. Figure 11 presents the results with two surrogates: pretrained model (f_{θ_0}) and model fine-tuned on (t = 1)Cars (f_{θ_1}) with $\gamma = \text{NI-FGSM}$ as the attack method. Clearly,

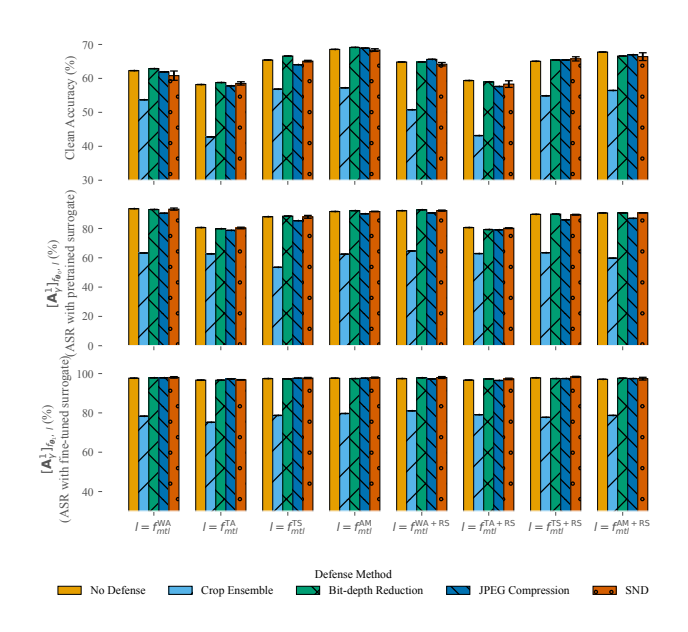


Fig. 11. Result of input transformation defenses. Here, $\gamma = \text{NI-FGSM}$

we observe no significant change in ASR for Bit-depth Reduction, JPEG Compression or SND. Therefore, these defenses prove to be ineffective. We do observe a modest drop in ASR for Crop Ensemble; however, not only is it computationally prohibitive since it requires multiple (30) inferences for a single image, it is also accompanied by significant drop in the model utility (clean accuracy), making the defense impractical.

Inspired from the literature, we suggest the following solution: Ghamizi et al. [70] observed weighing tasks during MTL helps increase adversarial robustness. Therefore, a penalty term can be added to the merging objective (cf. Eq. (1)) and tasks weighed to minimize transfer threat. Therefore, by trading a modest share of MTL accuracy for adversarial robustness, robust MM could be achieved. However, since higher target model test accuracy and decision boundary similarity are primary drivers of transferability [17], [20], [21], [73], we

conjecture that the core objectives of MM and low adversarial transferability may fundamentally be at odds with each other. We leave further exploration on this open for future research.

VIII. CONCLUSION

In this work, we identified MM—a widely adopted method within the machine learning community—cannot provide robustness against transfer attacks. Instead, we show that when stronger MM methods are employed, it increases a model's risk to transfer attacks. We statistically validate our empirical results, give theoretical explanations of the findings, and finally, discuss a potential solution to this problem. Our findings challenge the prevailing notion in the literature that MM confers adversarial robustness, and instead highlights a critical, previously overlooked vulnerability. By identifying this risk, we aim to advance the development of safer ML pipelines by understanding failure modes. We hope our work sparks future research in this important direction.

ETHICAL CONSIDERATIONS

Given the potential implications of our finding for deployed ML systems and user-facing applications, we have taken multiple steps to ensure the ethical handling and responsible dissemination of our results. All experiments were conducted in controlled environments using publicly available datasets and models. At no point did we target production systems, external APIs, or third-party applications. No sensitive, proprietary, or human-related data were involved in this study. We have adhered to standard ethical research guidelines to ensure that the dissemination of this work minimizes harm and promotes positive impact through increased model robustness and awareness.

REFERENCES

- [1] J. Devlin, M.-W. Chang, K. Lee, and K. Toutanova, "BERT: Pre-Training of Deep Bidirectional Transformers for Language Understanding," in Proceedings of the 2019 Conference of the North American Chapter of the Association for Computational Linguistics: Human Language Technologies, 2019, pp. 4171–4186.
- [2] C. Jia, Y. Yang, Y. Xia, Y.-T. Chen, Z. Parekh, H. Pham, Q. Le, Y.-H. Sung, Z. Li, and T. Duerig, "Scaling Up Visual and Vision-Language Representation Learning with Noisy Text Supervision," in *International Conference on Machine Learning*. PMLR, 2021, pp. 4904–4916.
- [3] A. Dosovitskiy, L. Beyer, A. Kolesnikov, D. Weissenborn, X. Zhai, T. Unterthiner, M. Dehghani, M. Minderer, G. Heigold, S. Gelly, J. Uszkoreit, and N. Houlsby, "An Image is Worth 16x16 Words: Transformers for Image Recognition at Scale," in *International Conference on Learning Representations*, 2021.
- [4] K. He, X. Zhang, S. Ren, and J. Sun, "Deep Residual Learning for Image Recognition," in *Proceedings of the IEEE Conference on Computer Vision and Pattern Recognition*, 2016, pp. 770–778.
- [5] A. Radford, J. W. Kim, C. Hallacy, A. Ramesh, G. Goh, S. Agarwal, G. Sastry, A. Askell, P. Mishkin, J. Clark et al., "Learning Transferable Visual Models from Natural Language Supervision," in *International Conference on Machine Learning*. PMLR, 2021, pp. 8748–8763.
- [6] R. Kemker, M. McClure, A. Abitino, T. Hayes, and C. Kanan, "Measuring Catastrophic Forgetting in Neural Networks," in *Proceedings of the AAAI Conference on Artificial Intelligence*, vol. 32, no. 1, 2018.
- [7] M. Wortsman, G. Ilharco, S. Y. Gadre, R. Roelofs, R. Gontijo-Lopes, A. S. Morcos, H. Namkoong, A. Farhadi, Y. Carmon, S. Kornblith et al., "Model Soups: Averaging Weights of Multiple Fine-Tuned Models Improves Accuracy Without Increasing Inference Time," in *International Conference On Machine Learning*. PMLR, 2022, pp. 23965–23998.

- [8] G. Ilharco, M. T. Ribeiro, M. Wortsman, L. Schmidt, H. Hajishirzi, and A. Farhadi, "Editing Models with Task Arithmetic," in *The Eleventh International Conference on Learning Representations*, 2023.
- [9] P. Yadav, D. Tam, L. Choshen, C. A. Raffel, and M. Bansal, "TIES-Merging: Resolving Interference When Merging Models," *Advances in Neural Information Processing Systems*, vol. 36, pp. 7093–7115, 2024.
- [10] E. Yang, Z. Wang, L. Shen, S. Liu, G. Guo, X. Wang, and D. Tao, "AdaMerging: Adaptive Model Merging for Multi-Task Learning," arXiv preprint:2310.02575, 2023.
- [11] E. Yang, L. Shen, Z. Wang, G. Guo, X. Chen, X. Wang, and D. Tao, "Representation Surgery for Multi-Task Model Merging," in *International Conference on Machine Learning*. PMLR, 2024, pp. 56332–56336
- [12] W. Junhao, Y. Zhe, and S. Jun, "Disrupting Model Merging: A Parameter-Level Defense Without Sacrificing Accuracy," arXiv preprint arXiv:2503.07661, 2025.
- [13] A. Arora, X. He, M. Mozes, S. Swain, M. Dras, and Q. Xu, "Here's a Free Lunch: Sanitizing Backdoored Models with Model Merge," in Findings of the Association for Computational Linguistics 2024, 2024, pp. 15059–15075.
- [14] C. Szegedy, "Intriguing Properties of Neural Networks," arXiv preprint:1312.6199, 2013.
- [15] J. Gu, X. Jia, P. de Jorge, W. Yu, X. Liu, A. Ma, Y. Xun, A. Hu, A. Khakzar, Z. Li, X. Cao, and P. Torr, "A Survey on Transferability of Adversarial Examples Across Deep Neural Networks," *Transactions on Machine Learning Research*, 2024.
- [16] N. Papernot, P. McDaniel, and I. Goodfellow, "Transferability in Machine Learning: From Phenomena to Black-Box Attacks using Adversarial Samples," arXiv preprint:1605.07277, 2016.
- [17] L. Wu and Z. Zhu, "Towards Understanding and Improving the Transferability of Adversarial Examples in Deep Neural Networks," in Asian Conference on Machine Learning, 2020, pp. 837–850.
- [18] N. Papernot, P. McDaniel, I. Goodfellow, S. Jha, Z. B. Celik, and A. Swami, "Practical Black-Box Attacks against Machine Learning," in *Proceedings of the 2017 ACM on Asia Conference on Computer and Communications Security*, 2017, pp. 506–519.
- [19] N. Carlini, A. Athalye, N. Papernot, W. Brendel, J. Rauber, D. Tsipras, I. Goodfellow, A. Madry, and A. Kurakin, "On Evaluating Adversarial Robustness," arXiv preprint arXiv:1902.06705, 2019.
- [20] F. Tramèr, N. Papernot, I. Goodfellow, D. Boneh, and P. McDaniel, "The Space of Transferable Adversarial Examples," arXiv preprint arXiv:1704.03453, 2017.
- [21] Y. Liu, X. Chen, C. Liu, and D. Song, "Delving into Transferable Adversarial Examples and Black-box Attacks," in *International Conference on Learning Representations*, 2017.
- [22] I. J. Goodfellow, J. Shlens, and C. Szegedy, "Explaining and Harnessing Adversarial Examples," arXiv preprint arXiv:1412.6572, 2014.
- [23] A. Kurakin, I. J. Goodfellow, and S. Bengio, "Adversarial Examples in the Physical World," in *Artificial Intelligence Safety and Security*. Chapman and Hall/CRC, 2018, pp. 99–112.
- [24] A. Madry, A. Makelov, L. Schmidt, D. Tsipras, and A. Vladu, "Towards Deep Learning Models Resistant to Adversarial Attacks," in *Interna*tional Conference on Learning Representations, 2018.
- [25] J. Lin, C. Song, K. He, L. Wang, and J. E. Hopcroft, "Nesterov Accelerated Gradient and Scale Invariance for Adversarial Attacks," in International Conference on Learning Representations, 2019.
- [26] Y. Dong, T. Pang, H. Su, and J. Zhu, "Evading Defenses to Transferable Adversarial Examples by Translation-Invariant Attacks," in *Proceedings* of the IEEE/CVF Conference on Computer Vision and Pattern Recognition, 2019, pp. 4312–4321.
- [27] M. Andriushchenko, F. Croce, N. Flammarion, and M. Hein, "Square Attack: A Query-Efficient Black-Box Adversarial Attack via Random Search," in *European Conference on Computer Vision*. Springer, 2020, pp. 484–501.
- [28] M. Li, C. Deng, T. Li, J. Yan, X. Gao, and H. Huang, "Towards Transferable Targeted Attack," in *Proceedings of the IEEE/CVF Conference on Computer Vision and Pattern Recognition*, 2020, pp. 641–649.
- [29] A. Paszke, S. Gross, F. Massa, A. Lerer, J. Bradbury, G. Chanan, T. Killeen, Z. Lin, N. Gimelshein, L. Antiga, A. Desmaison, A. Kopf, E. Yang, Z. DeVito, M. Raison, A. Tejani, S. Chilamkurthy, B. Steiner, L. Fang, J. Bai, and S. Chintala, "PyTorch: An Imperative Style, High-Performance Deep Learning Library," in Advances in Neural Information Processing Systems, vol. 32. Curran Associates, Inc., 2019.

- [30] D. P. Kingma and J. Ba, "Adam: A Method for Stochastic Optimization," arXiv preprint arXiv:1412.6980, 2014.
- [31] J. Krause, M. Stark, J. Deng, and L. Fei-Fei, "3D Object Representations for Fine-Grained Categorization," in *ICCV Workshops*, 2013, pp. 554– 561
- [32] Y. LeCun, "The MNSIT Database Of Handwritten Digits," http://yann. lecun. com/exdb/mnist/, 1998.
- [33] P. Helber, B. Bischke, A. Dengel, and D. Borth, "EuroSAT: A Novel Dataset and Deep Learning Benchmark for Land Use and Land Cover Classification," *IEEE Journal of Selected Topics in Applied Earth Observations and Remote Sensing*, pp. 2217–2226, 2019.
- [34] J. Stallkamp, M. Schlipsing, J. Salmen, and C. Igel, "The German Traffic Sign Recognition Benchmark: A Multi-Class Classification Competition," in *IJCNN*. IEEE, 2011, pp. 1453–1460.
- [35] N. Yuval, "Reading Digits in Natural Images with Unsupervised Feature Learning," in NIPS Workshop, 2011.
- [36] G. Cheng, J. Han, and X. Lu, "Remote Sensing Image Scene Classification: Benchmark and State of the Art," *Proceedings of the IEEE*, vol. 105, no. 10, pp. 1865–1883, 2017.
- [37] M. Cimpoi, S. Maji, I. Kokkinos, S. Mohamed, and A. Vedaldi, "Describing Textures in The Wild," in CVPR, 2014, pp. 3606–3613.
- [38] K. He, X. Zhang, S. Ren, and J. Sun, "Deep residual learning for image recognition," in *Proceedings of the IEEE Conference on Computer Vision And Pattern Recognition*, 2016, pp. 770–778.
- [39] A. Athalye, N. Carlini, and D. Wagner, "Obfuscated Gradients Give a False Sense of Security: Circumventing Defenses to Adversarial Examples," in *International Conference On Machine Learning*. PMLR, 2018, pp. 274–283.
- [40] N. J. Salkind, Encyclopedia of Research Design. SAGE, 2010, vol. 1.
- [41] Student, "The Probable Error of a Mean," Biometrika, pp. 1-25, 1908.
- [42] F. Wilcoxon, "Individual Comparisons by Ranking Methods," in *Breakthroughs in Statistics: Methodology and Distribution*. Springer, 1992, pp. 196–202.
- [43] S. S. Shapiro and M. B. Wilk, "An Analysis of Variance Test for Normality (Complete Samples)," *Biometrika*, vol. 52, no. 3-4, pp. 591– 611, 1965.
- [44] Y. Benjamini and Y. Hochberg, "Controlling the False Discovery Rate: A Practical and Powerful Approach to Multiple Testing," *Journal of The Royal Statistical Society: Series B (Methodological)*, vol. 57, no. 1, pp. 289–300, 1995.
- [45] J. Cohen, Statistical Power Analysis for The Behavioral Sciences. Routledge, 2013.
- [46] M. Tomczak and E. Tomczak, "The Need to Report Effect Size Estimates Revisited. An Overview of Some Recommended Measures of Effect Size," *Trends in Sport Sciences*, vol. 21, no. 1, pp. 19–25, 2014.
- [47] N. L. Kerr, "HARKing: Hypothesizing After the Results are Known," Personality and Social Psychology Review, vol. 2, no. 3, pp. 196–217, 1998.
- [48] J. Frankle, G. K. Dziugaite, D. Roy, and M. Carbin, "Linear Mode Connectivity and the Lottery Ticket Hypothesis," in *International Conference on Machine Learning*, 2020, pp. 3259–3269.
- [49] P. Izmailov, D. Podoprikhin, T. Garipov, D. Vetrov, and A. G. Wilson, "Averaging Weights Leads to Wider Optima and Better Generalization," in 34th Conference on Uncertainty in Artificial Intelligence, 2018, pp. 876–885.
- [50] B. Neyshabur, H. Sedghi, and C. Zhang, "What is Being Transferred in Transfer Learning?" Advances in Neural Information Processing Systems, vol. 33, pp. 512–523, 2020.
- [51] G. Ilharco, M. Wortsman, S. Y. Gadre, S. Song, H. Hajishirzi, S. Kornblith, A. Farhadi, and L. Schmidt, "Patching Open-Vocabulary Models by Interpolating Weights," *Advances in Neural Information Processing Systems*, vol. 35, pp. 29 262–29 277, 2022.
- [52] Z. Zhou, Y. Yang, X. Yang, J. Yan, and W. Hu, "Going Beyond Linear Mode Connectivity: The Layerwise Linear Feature Connectivity," Advances in Neural Information Processing Systems, vol. 36, pp. 60853–60877, 2023.
- [53] Z. Zhou, Z. Chen, Y. Chen, B. Zhang, and J. Yan, "On The Emergence of Cross-Task Linearity in Pretraining-Finetuning Paradigm," in Proceedings of the 41st International Conference on Machine Learning, 2024, pp. 61854–61884.
- [54] M. S. Matena and C. A. Raffel, "Merging Models with Fisher-Weighted Averaging," Advances in Neural Information Processing Systems, vol. 35, pp. 17703–17716, 2022.

- [55] X. Jin, X. Ren, D. Preotiuc-Pietro, and P. Cheng, "Dataless Knowledge Fusion by Merging Weights of Language Models," in *International Conference on Learning Representations*, 2022.
- [56] T. Li, Z. Huang, Q. Tao, Y. Wu, and X. Huang, "Trainable Weight Averaging: Efficient Training by Optimizing Historical Solutions," in International Conference on Learning Representations, 2022.
- [57] J. Zhang, J. Liu, J. He et al., "Composing Parameter-Efficient Modules with Arithmetic Operation," Advances in Neural Information Processing Systems, vol. 36, pp. 12589–12610, 2023.
- [58] C. Huang, Q. Liu, B. Y. Lin, T. Pang, C. Du, and M. Lin, "LoraHub: Efficient Cross-Task Generalization via Dynamic Lora Composition," arXiv preprint arXiv:2307.13269, 2023.
- [59] A. Rame, G. Couairon, C. Dancette, J.-B. Gaya, M. Shukor, L. Soulier, and M. Cord, "Rewarded Soups: Towards Pareto-Optimal Alignment by Interpolating Weights Fine-Tuned on Diverse Rewards," Advances in Neural Information Processing Systems, vol. 36, pp. 71095–71134, 2024.
- [60] J. Li, J. Cho, Y.-L. Sung, J. Yoon, and M. Bansal, "SELMA: Learning and Merging Skill-Specific Text-to-Image Experts with Auto-Generated Data," arXiv preprint arXiv:2403.06952, 2024.
- [61] N. G. Nair, J. M. J. Valanarasu, and V. M. Patel, "MaxFusion: Plug&Play Multi-Modal Generation In Text-To-Image Diffusion Models," in European Conference on Computer Vision. Springer, 2024, pp. 93–110.
- [62] J. Zhang, J. Chi, Z. Li, K. Cai, Y. Zhang, and Y. Tian, "BadMerging: Backdoor Attacks Against Model Merging," in *Proceedings of the* 2024 on ACM SIGSAC Conference on Computer and Communications Security, 2024, pp. 4450–4464.
- [63] L. Wang, J. Wang, T. Cong, X. He, Z. Qin, and X. Huang, "From Purity to Peril: Backdooring Merged Models From "Harmless" Benign Components," in USENIX Security Symposium (USENIX Security), 2025.
- [64] Z. Yuan, Y. Xu, J. Shi, P. Zhou, and L. Sun, "Merge Hijacking: Backdoor Attacks to Model Merging of Large Language Models," in *Proceedings* of the 63rd Annual Meeting of the Association for Computational Linguistics (Volume 1: Long Papers), 2025, pp. 32688–32703.
- [65] A. Gangwal and A. A. Sharma, "POSTER: Investigating Transferability of Adversarial Examples in Model Merging," in *Proceedings of the* 20th ACM Asia Conference on Computer and Communications Security, 2025, pp. 1812–1814.
- [66] A. Demontis, M. Melis, M. Pintor, M. Jagielski, B. Biggio, A. Oprea, C. Nita-Rotaru, and F. Roli, "Why Do Adversarial Attacks Transfer? Explaining Transferability of Evasion and Poisoning Attacks," in 28th USENIX security symposium (USENIX Security 19), 2019, pp. 321–338.
- [67] H. B. Mann and D. R. Whitney, "On a Test of Whether One of Two Random Variables Is Stochastically Larger than the Other," *The Annals of Mathematical Statistics*, pp. 50–60, 1947.
- [68] C. Mao, A. Gupta, V. Nitin, B. Ray, S. Song, J. Yang, and C. Vondrick, "Multitask learning strengthens adversarial robustness," in 16th European Conference on Computer Vision (ECCV). Springer, 2020, pp. 158–174.
- [69] L. Zhang, X. Liu, K. Mahmood, C. Ding, and H. Guan, "Multi-Task Models Adversarial Attacks," arXiv preprint arXiv:2305.12066, 2023.
- [70] S. Ghamizi, M. Cordy, M. Papadakis, and Y. Le Traon, "Adversarial Robustness in Multi-Task Learning: Promises and Illusions," in *Proceedings of the AAAI Conference on Artificial Intelligence*, vol. 36, no. 1, 2022, pp. 697–705.
- [71] C. Guo, M. Rana, M. Cisse, and L. van der Maaten, "Countering Adversarial Images using Input Transformations," in *International Conference on Learning Representations*, 2018.
- [72] J. Byun, H. Go, and C. Kim, "On the Effectiveness of Small Input Noise for Defending Against Query-based Black-Box Attacks," in *Proceedings* of the IEEE/CVF Winter Conference on Applications of Computer Vision, 2022, pp. 3051–3060.
- [73] F. Waseda, S. Nishikawa, T.-N. Le, H. H. Nguyen, and I. Echizen, "Closer Look at the Transferability of Adversarial Examples: How They Fool Different Models Differently," in *Proceedings of the IEEE/CVF Winter Conference on Applications of Computer Vision*, 2023, pp. 1360–1368.
- [74] N. Yuval, "Reading Digits in Natural Images with Unsupervised Feature Learning," in NIPS Workshop, 2011.

ORGANIZATION OF APPENDIX

In Appendix A, we provide the description of the attack used in our work. Appendix B provides the experiment and hyperparameter details omitted from the main text. Appendix C details the proof alluded in \$VII-B. Appendix D provides the statistical tests per each attack method for \mathcal{H}_1 and \mathcal{H}_3 , omitted in \$V-A and \$V-C for brevity. Appendix E provides the ASR matrices for other attack methods that were omitted due to page limitations. Appendix F provides the ASR matrices for targeted attack mentioned in \$VII-C. Appendix G provides the ASR matrices for the attack setting in which adversary uses CLIP ResNet-50 as the surrogate, i.e., surrogate with different architecture than the merged model mentioned in \$VII-E. Appendix H provides result on query-based (SQUARE) attack on the target models, mentioned in \$VII-D.

APPENDIX A DESCRIPTION OF THE ATTACK USED IN OUR WORK

1) Fast Gradient Sign Method (FGSM) [22]. FGSM is a one-step method that generates an adversarial perturbation using the sign of the gradient of the loss function \mathcal{L} with respect to the input:

$$\tilde{\mathbf{x}}_i = \mathbf{x}_i + \epsilon \cdot \operatorname{sign}(\nabla_{\mathbf{x}_i} \mathcal{L}(f_{\theta}(\mathbf{x}_i), \mathbf{y}_i)). \tag{A.1}$$

2) **Iterative FGSM** (**I-FGSM**) [23]. I-FGSM, a.k.a. Basic Iterative Method (BIM) improves upon FGSM by applying it iteratively with a small step size α_{γ} and clipping the result after each step to keep it within the ϵ -ball of the original input. Formally, after initialization $\tilde{\mathbf{x}}_i^{(0)} = \mathbf{x}_i$, $\tilde{\mathbf{x}}_i^k$ is updated to $\tilde{\mathbf{x}}_i^{k+1}$ as:

$$\operatorname{Clip}_{\mathbf{x}_{i},\epsilon} \left\{ \tilde{\mathbf{x}}_{i}^{(k)} + \alpha_{\gamma} \cdot \operatorname{sign}(\nabla_{\tilde{\mathbf{x}}_{i}^{(k)}} \mathcal{L}(f_{\theta}(\tilde{\mathbf{x}}_{i}^{(k)}), \mathbf{y}_{i})) \right\}. \tag{A.2}$$

3) **Projected Gradient Descent (PGD) [24].** PGD extends I-FGSM by introducing random initialization and re-projecting the perturbed example onto the ϵ -ball around the original input after each update step. Specifically, starting from $\tilde{\mathbf{x}}_i^{(0)} = \mathbf{x}_i + \mathcal{U}(-\epsilon, \epsilon)$ (uniform noise within the ϵ -ball), $\tilde{\mathbf{x}}_i^{(k)}$ is updated to $\tilde{\mathbf{x}}_i^{(k+1)}$ as follows:

$$\mathcal{B}_{\mathbf{x}_{i},\epsilon} \left\{ \tilde{\mathbf{x}}_{i}^{(k)} + \alpha_{\gamma} \cdot \operatorname{sign}(\nabla_{\tilde{\mathbf{x}}_{i}^{(k)}} \mathcal{L}(f_{\boldsymbol{\theta}}(\tilde{\mathbf{x}}_{i}^{(k)}), \mathbf{y}_{i})) \right\}, \tag{A.3}$$

where $\mathcal{B}_{\mathbf{x}_i,\epsilon}(\cdot)$ projects the perturbed input back into the ℓ_p ball of radius ϵ centered at \mathbf{x}_i . When initialized at \mathbf{x}_i (i.e., without random noise) with ℓ_{∞} -norm constraint, PGD reduces to I-FGSM.

4) Nesterov Iterative FGSM (NI-FGSM) [25]. NI-FGSM incorporates momentum and a Nesterov-like lookahead gradient to stabilize and accelerate updates. Let $\mathbf{g}^{(k)}$ and μ_d be the accumulated gradient at step k and the decay factor, respectively. Then $\mathbf{g}^{(k+1)}$ and $\tilde{\mathbf{x}}_i^{(k+1)}$ will be equal to:

$$\mu_d \cdot \mathbf{g}^{(k)} + \frac{\nabla_{\mathbf{x}} \mathcal{L}(f_{\boldsymbol{\theta}}(\mathbf{x}_i + \alpha_{\gamma} \cdot \mu \cdot \mathbf{g}^{(k)}), \mathbf{y}_i)}{\|\nabla_{\mathbf{x}} \mathcal{L}(f_{\boldsymbol{\theta}}(\mathbf{x}_i + \alpha_{\gamma} \cdot \mu \cdot \mathbf{g}^{(k)}), \mathbf{y}_i))\|_1},\tag{A.4}$$

$$\tilde{\mathbf{x}}_{i}^{(k+1)} = \operatorname{Clip}_{\mathbf{x}_{i}, \epsilon} \left\{ \tilde{\mathbf{x}}_{i}^{(k)} + \alpha_{\gamma} \cdot \operatorname{sign}(\mathbf{g}^{(k+1)}) \right\}. \tag{A.5}$$

5) **Translation-Invariant FGSM** (**TI-FGSM**) [26]. TI-FGSM enhances transferability by convolving the gradient with a fixed smoothing kernel (typically Gaussian) before applying FGSM-like updates. Let **W** be the convolution kernel, then:

$$\tilde{\mathbf{x}}_i = \mathbf{x}_i + \epsilon \cdot \text{sign} \left(\mathbf{W} * \nabla_{\mathbf{x}_i} \mathcal{L}(f_{\theta}(\mathbf{x}_i), \mathbf{y}_i) \right), \tag{A.6}$$

where * denotes convolution. The iterative variant of TI-FGSM is obtained by including the convolution kernel **W** in Eq. (A.2). Consequently, $\tilde{\mathbf{x}}_i^{(k)}$ will be updated to $\tilde{\mathbf{x}}_i^{(k+1)}$ as:

$$\operatorname{Clip}_{\mathbf{x}_{i},\epsilon} \left\{ \tilde{\mathbf{x}}_{i}^{(k)} + \alpha_{\gamma} \cdot \operatorname{sign}(\mathbf{W} * \nabla_{\tilde{\mathbf{x}}_{i}^{(k)}} \mathcal{L}(f_{\boldsymbol{\theta}}(\tilde{\mathbf{x}}_{i}^{(k)}), \mathbf{y}_{i})) \right\}. \tag{A.7}$$

6) Square Attack [27]. Square Attack is a score-based black-box adversarial method that does not rely on gradient information and remains effective even under gradient masking. It performs a randomized search by iteratively applying localized square-shaped perturbations within the ℓ_p threat model $(p \in \{2, \infty\})$. At each iteration, it samples a square region of the input, adds a perturbation lying on the boundary of the ℓ_p ball of radius ϵ , and accepts the update if it increases the attack loss. This strategy efficiently explores the perturbation space and achieves high success rates with significantly fewer model queries compared to prior black-box methods, for both ℓ_∞ and ℓ_2

APPENDIX B EXPERIMENTAL DETAILS

A. Datasets

Following prior work on TA [8], TM [9], AM [10] and RS [11], we conducted our experiments on the following seven benchmark datasets:

- Cars [31]. The Stanford Cars dataset consists of 16,185 images from 196 car classes, split equally between training and test sets.
- **RESISC45** [36]. A remote sensing scene classification benchmark with 45 classes, each containing 700 images (256×256 resolution), totaling 31,500 images.
- EuroSAT [33]. A geospatial land use dataset containing 27,000 Sentinel-2 satellite images annotated into 10 classes.
- SVHN [74]. The Street View House Numbers dataset comprises over 600,000 real-world color images of house numbers, divided into 10 classes.
- GTSRB [34]. The German Traffic Sign Recognition Benchmark features more than 50,000 images in 43 classes, exhibiting
 diverse lighting and background conditions.
- MNIST [32]. A widely used dataset of 70,000 grayscale images of handwritten digits in 10 classes, with 60,000 for training and 10,000 for testing (28×28 resolution).
- **DTD** [37]. The Describable Textures Dataset contains 5,640 labeled texture images across 47 categories, with approximately 120 images per class (ranging from 300×300 to 640×640 pixels).

B. Hyperparameters

We follow prior works [26], [25] and set the perturbation budget ϵ , step size α_{γ} and number of iteration t_{γ} to 16/255, 1.6/255 and 10 to generate adversarial examples. For NI-FGSM, we use the default decay factor $\mu_d=1$. However, we observed degraded performance in case of MNIST with this configuration, since it is a single-channel dataset, as opposed to other datasets, which are three-channel. Therefore, we follow Madry et al. [24] and choose $\epsilon=0.3$, $\alpha_{\gamma}=0.03$ and $t_{\gamma}=10$ for MNIST. In line with the original implementation of TI-FGSM, we choose the Gaussian kernel with kernel size k=15 and standard deviation $\sigma=\frac{k}{\sqrt{3}}$. For Square attack, we fix query budget to 500 and size of square p=0.8. Finally, for targeted attacks, we randomly select the label to perform targeted attacks. We follow experimental setup of RS [11] to obtain RS-augmented merged models, and run all experiments for 500 iterations with a batch size of 16. The rank for the adapter module is set to 16 by default. We obtain the pretrained ResNet-50 model from open_clip library, and fine-tune the model for 10 epochs. We set the base learning rate to 10^{-3} , encoder learning rate to 10^{-4} , with the weight decay 0.1. Finally, we use AdamW as the optimizer, clip gradients to a max norm of 1.0, and use cross-entropy as the loss.

APPENDIX C

Lemma 1 (Direction that maximizes average cosine similarity). Let $v_1, \ldots, v_T \in \mathbb{R}^d$ be nonzero vectors and define the unit directions $w_t \coloneqq v_t/\|v_t\|$ and their mean $\bar{w} \coloneqq \frac{1}{T} \sum_{t=1}^T w_t$. For any nonzero $x \in \mathbb{R}^d$, the average cosine similarity

$$F(x) := \frac{1}{T} \sum_{t=1}^{T} \cos(x, v_t) = \frac{1}{T} \sum_{t=1}^{T} \frac{\langle x, v_t \rangle}{\|x\| \|v_t\|}$$

satisfies

$$F(x) \; = \; \left\langle \frac{x}{\|x\|}, \, \bar{w} \right\rangle \; \leq \; \|\bar{w}\|$$

with equality if and only if x is a positive scalar multiple of \bar{w} whenever $\bar{w} \neq 0$. Consequently, every maximizer has direction of \bar{w} , and the maximum value of F equals $\|\bar{w}\|$. If $\bar{w} = 0$, then F(x) = 0 for all $x \neq 0$.

Proof. Since $v_t \neq 0$, we can write $v_t = ||v_t|| w_t$ with $||w_t|| = 1$. Then

$$F(x) = \frac{1}{T} \sum_{t=1}^{T} \frac{\langle x, ||v_t|| w_t \rangle}{||x|| ||v_t||} = \left\langle \frac{x}{||x||}, \frac{1}{T} \sum_{t=1}^{T} w_t \right\rangle = \left\langle \frac{x}{||x||}, \bar{w} \right\rangle.$$

By Cauchy–Schwarz, $\langle x/\|x\|, \bar{w} \rangle \leq \|x/\|x\| \|\|\bar{w}\| = \|\bar{w}\|$, with equality iff $x/\|x\|$ is parallel to \bar{w} and with nonnegative alignment at the maximizer. This yields the claim above. If $\bar{w} = 0$, then F(x) = 0 for all $x \neq 0$.

Corollary 1 (Unit-vector case). If each v_t is unit, then $w_t = v_t$ and $\bar{w} = \frac{1}{T} \sum_{t=1}^T v_t$. The unit maximizer is $x^* = \bar{w}/\|\bar{w}\|$ when $\bar{w} \neq 0$, and the maximum equals $\|\bar{w}\|$.

Corollary 2 (Application to Eq. (38)). Let $g_t(\mathbf{x}) \coloneqq \nabla_{\mathbf{x}} \mathcal{L}(f_{\theta_t}(\mathbf{x}), \mathbf{y})$ and suppose

$$abla_{\mathbf{x}} \mathcal{L}ig(f_{oldsymbol{ heta}_{mtl}}(\mathbf{x}), \mathbf{y}ig) \; pprox \; rac{1}{T} \sum_{t=1}^{T} rac{g_t(\mathbf{x})}{\|g_t(\mathbf{x})\|},$$

as stated in Eq. (38). Then by the lemma, the WA gradient direction approximately maximizes the average cosine similarity with the individual gradients $\{g_t(\mathbf{x})\}_{t=1}^T$, and the maximal average cosine is approximately the norm of the average of the normalized gradients.

$\label{eq:APPENDIX D} \text{Results for Per Attack Samples for \mathcal{H}_1 and \mathcal{H}_3}$

A. Result for \mathcal{H}_1

TABLE D.1
STATISTICAL TEST RESULTS COMPARING ADAMERGING WITH TA AND TIES UNDER DIFFERENT ATTACKS, REPORTED WITHOUT RS (SIMPLE) AND WITH RS (SURGERY).

Sample	Test Used	Test Statistic	One-tailed p-value	BH-corrected p-value	Effect Size
		Simple	: TA vs AdaMerging		
$\mathring{\Delta}_{\mathrm{AM, TA}}^{\mathrm{FGSM}}$	t-test	$t_s = 4.992$	1.23×10^{-4}	3.08×10^{-4}	d = 1.334
$\mathring{\Delta}_{AM}^{I-FGSM}$	Wilcoxon	W = 104.0	1.22×10^{-4}	3.08×10^{-4}	r = 0.864
$\mathring{\Delta}_{\mathrm{AM, TA}}^{\mathrm{PGD}}$	t-test	$t_s = 3.849$	1.01×10^{-3}	1.26×10^{-3}	d = 1.029
$\mathring{oldsymbol{\Delta}}_{ ext{AM, TA}}^{ ext{NI-FGSM}}$	t-test	$t_s = 0.895$	1.94×10^{-1}	1.94×10^{-1}	d = 0.239
$\mathring{m{\Delta}}_{ ext{AM, TA}}^{ ext{TI-FGSM}}$	t-test	$t_s = 4.725$	1.99×10^{-4}	3.31×10^{-4}	d = 1.263
		Simple:	TIES vs AdaMerging	ţ	
$\mathring{f\Delta}_{ m AM,TM}^{ m FGSM}$	t-test	$t_s = 0.730$	2.39×10^{-1}	3.98×10^{-1}	d = 0.195
$\mathring{\Delta}_{\mathrm{AM}}^{\mathrm{I-FGSM}}$	Wilcoxon	W = 65.0	2.32×10^{-1}	3.98×10^{-1}	r = 0.210
$\mathring{\Delta}_{\mathrm{AM,TM}}^{\mathrm{PGD}}$	Wilcoxon	W = 67.0	1.96×10^{-1}	3.98×10^{-1}	r = 0.243
$\mathring{\Delta}_{ ext{AM, TM}}^{ ext{NI-FGSM}}$	Wilcoxon	W = 54.0	4.63×10^{-1}	5.36×10^{-1}	r = 0.025
$\mathring{\Delta}_{ ext{AM, TM}}^{ ext{TI-FGSM}}$	t-test	$t_s = -0.092$	5.36×10^{-1}	5.36×10^{-1}	d = -0.024
		Surger	y: TA vs AdaMerging		
$\mathring{\mathbf{\Delta}}_{\mathrm{AM+RS, TA+RS}}^{\mathrm{FGSM}}$	t-test	$t_s = 3.486$	2.01×10^{-3}	2.47×10^{-3}	d = 0.932
$\mathring{\Delta}_{\text{AM+RS, TA+RS}}^{\text{I-FGSM}}$	Wilcoxon	W = 105.0	6.10×10^{-5}	1.53×10^{-4}	r = 0.881
$\Delta_{\text{AM+RS, TA+RS}}^{\text{rGD}}$	Wilcoxon	W = 105.0	6.10×10^{-5}	1.53×10^{-4}	r = 0.881
$\mathring{\Delta}_{\text{AM+RS, TA+RS}}^{\text{NI-FGSM}}$	t-test	$t_s = 3.379$	2.47×10^{-3}	2.47×10^{-3}	d = 0.903
$\mathring{\Delta}_{ ext{AM+RS, TA+RS}}^{ ext{TI-FGSM}}$	t-test	$t_s = 5.151$	9.32×10^{-5}	1.55×10^{-4}	d = 1.377
		Surgery	: TIES vs AdaMergin	g	
$\mathring{\Delta}_{\text{AM+RS. TM+RS}}^{\text{FGSM}}$	t-test	$t_s = -1.134$	8.61×10^{-1}	8.61×10^{-1}	d = -0.303
$\mathring{\Delta}_{\text{AM+RS, TM+RS}}^{\text{I-FGSM}}$	Wilcoxon	W = 57.0	4.04×10^{-1}	5.05×10^{-1}	r = 0.075
$\mathring{\mathbf{\Delta}}_{\mathrm{AM+RS,TM+RS}}^{\mathrm{PGD}}$	Wilcoxon	W = 70.0	1.48×10^{-1}	2.50×10^{-1}	r = 0.294
$\mathring{\Delta}_{\mathrm{AM+RS,TM+RS}}^{\mathrm{NI-FGSM}}$	Wilcoxon	W = 69.0	1.50×10^{-1}	2.50×10^{-1}	r = 0.277
$\mathring{\Delta}^{\text{TI-FGSM}}_{\text{AM+RS, TM+RS}}$	Wilcoxon	W = 71.0	1.34×10^{-1}	2.50×10^{-1}	r = 0.310

 $\begin{array}{c} \text{TABLE D.2} \\ \text{Statistical test results for } \hat{\mathbf{\Delta}}_{\text{WA, TA}}^{\gamma}, \hat{\mathbf{\Delta}}_{\text{WA, TM}}^{\gamma}, \, \hat{\mathbf{\Delta}}_{\text{WA, AM}}^{\gamma} \, \forall \, \gamma \in \Gamma. \end{array}$

Sample	Test Used	Test Statistic	One-tailed p-value	BH-corrected p-value	Effect Size
$\mathring{\mathbf{\Delta}}_{\mathrm{WA, TA}}^{\mathrm{FGSM}}$	Wilcoxon	$W = 6.10 \times 10^{-5}$	1.83×10^{-4}	1.83×10^{-4}	r = 0.8808
$\mathring{\Delta}_{\mathrm{WA,TM}}^{\mathrm{FGSM}}$	t-test	$t_s = 5.91 \times 10^{-4}$	8.87×10^{-4}	8.87×10^{-4}	d = 0.3051
$\mathring{\Delta}_{ ext{WA, AM}}^{ ext{FGSM}}$	t-test	$t_s = 4.58 \times 10^{-2}$	4.58×10^{-2}	4.58×10^{-2}	d = 0.2498
$\mathring{\Delta}_{\mathrm{WA, TA}}^{\mathrm{I-FGSM}}$	t-test	$t_s = 2.48 \times 10^{-3}$	7.43×10^{-3}	7.43×10^{-3}	d = 0.6926
$\mathring{\Delta}_{\mathrm{WA,TM}}^{\mathrm{I-FGSM}}$	Wilcoxon	$W = 1.76 \times 10^{-2}$	2.65×10^{-2}	2.65×10^{-2}	r = 0.5621
$\mathring{\Delta}_{ ext{WA, AM}}^{ ext{I-FGSM}}$	Wilcoxon	$W = 7.60 \times 10^{-2}$	7.60×10^{-2}	7.60×10^{-2}	r = 0.3973
$\mathring{oldsymbol{\Delta}}_{ ext{WA, TA}}^{ ext{PGD}}$	t-test	$t_s = 2.23 \times 10^{-3}$	6.69×10^{-3}	6.69×10^{-3}	d = 0.7436
$\mathring{\Delta}_{ ext{WA, TM}}^{ ext{PGD}}$	Wilcoxon	$W=1.48\times 10^{-2}$	2.22×10^{-2}	2.22×10^{-2}	r = 0.5788
$\mathring{oldsymbol{\Delta}}_{ ext{WA, AM}}^{ ext{PGD}}$	Wilcoxon	$W = 5.47 \times 10^{-2}$	5.47×10^{-2}	5.47×10^{-2}	r = 0.4278
$\mathring{\Delta}_{ ext{WA, TA}}^{ ext{NI-FGSM}}$	Wilcoxon	$W=2.62\times 10^{-3}$	7.87×10^{-3}	7.87×10^{-3}	r = 0.7131
$\mathring{\Delta}_{ ext{WA, TM}}^{ ext{NI-FGSM}}$	t-test	$t_s = 1.08 \times 10^{-2}$	1.62×10^{-2}	1.62×10^{-2}	d = 0.2569
$\mathring{\Delta}_{ ext{WA, AM}}^{ ext{NI-FGSM}}$	Wilcoxon	$W = 5.20 \times 10^{-2}$	5.20×10^{-2}	5.20×10^{-2}	r = 0.4446
$\mathring{\Delta}_{\mathrm{WA, TA}}^{\mathrm{TI-FGSM}}$	t-test	$t_s = 1.36 \times 10^{-3}$	4.08×10^{-3}	4.08×10^{-3}	d = 0.5719
$\mathring{\Delta}_{\mathrm{WA,TM}}^{\mathrm{TI-FGSM}}$	t-test	$t_s = 6.22 \times 10^{-3}$	9.34×10^{-3}	9.34×10^{-3}	d = 0.3537
$\mathring{\Delta}_{\mathrm{WA,AM}}^{\mathrm{TI-FGSM}}$	Wilcoxon	$W = 3.94 \times 10^{-2}$	3.94×10^{-2}	3.94×10^{-2}	r = 0.4698

 $\begin{array}{c} \text{TABLE D.3} \\ \text{Statistical test results for } \mathring{\Delta}_{WA+RS, \; TA+RS}^{\gamma}, \mathring{\Delta}_{WA+RS, \; TM+RS}^{\gamma}, \mathring{\Delta}_{WA+RS, \; AM+RS}^{\gamma} \; \forall \; \gamma \in \Gamma. \end{array}$

Sample	Test Used	Test Statistic	One-tailed p-value	BH-corrected p-value	Effect Size
ÅFGSM WA+RS, TA+RS ÅFGSM WA+RS, TM+RS ÅFGSM WA+RS, AM+RS	t-test t-test t-test	8.63×10^{-3} 4.83×10^{-1} 2.17×10^{-1}	2.59×10^{-2} 4.83×10^{-1} 3.25×10^{-1}	2.59×10^{-2} 4.83×10^{-1} 3.25×10^{-1}	d = 0.4944 $d = 0.0054$ $d = 0.0843$
$\mathring{\Delta}_{WA+RS, TA+RS}^{I-FGSM}$ $\mathring{\Delta}_{WA+RS, TM+RS}^{I-FGSM}$ $\mathring{\Delta}_{WA+RS, TM+RS}^{I-FGSM}$ $\mathring{\Delta}_{WA+RS, AM+RS}^{I-FGSM}$	t-test t-test Wilcoxon	1.32×10^{-3} 6.65×10^{-3} 5.94×10^{-2}	3.95×10^{-3} 9.98×10^{-3} 5.94×10^{-2}	3.95×10^{-3} 9.98×10^{-3} 5.94×10^{-2}	d = 0.6095 $d = 0.2793$ $r = 0.4278$
$\mathring{\Delta}_{WA+RS, TA+RS}^{PGD}$ $\mathring{\Delta}_{WA+RS, TM+RS}^{PGD}$ $\mathring{\Delta}_{WA+RS, TM+RS}^{PGD}$ $\mathring{\Delta}_{WA+RS, AM+RS}^{PGD}$	Wilcoxon t-test Wilcoxon	1.53×10^{-3} 3.78×10^{-3} 4.53×10^{-2}	4.58×10^{-3} 5.67×10^{-3} 4.53×10^{-2}	4.58×10^{-3} 5.67×10^{-3} 4.53×10^{-2}	r = 0.7466 d = 0.3046 r = 0.4614
ÅNI-FGSM WA+RS, TA+RS ÅNI-FGSM WA+RS, TM+RS ÅNI-FGSM WA+RS, AM+RS	Wilcoxon Wilcoxon Wilcoxon	4.27×10^{-3} 5.94×10^{-2} 1.76×10^{-2}	1.28×10^{-2} 5.94×10^{-2} 2.65×10^{-2}	1.28×10^{-2} 5.94×10^{-2} 2.65×10^{-2}	r = 0.6795 r = 0.4278 r = 0.5621
ÅTI-FGSM WA+RS, TA+RS ÅTI-FGSM WA+RS, TM+RS ÅTI-FGSM WA+RS, AM+RS	t-test t-test t-test	8.12×10^{-4} 7.28×10^{-3} 2.61×10^{-2}	2.44×10^{-3} 1.09×10^{-2} 2.61×10^{-2}	2.44×10^{-3} 1.09×10^{-2} 2.61×10^{-2}	d = 0.4433 $d = 0.2342$ $d = 0.2085$

APPENDIX E ASR MATRICES

TABLE E.1 ASR matrices $(\{\mathbf{A}_{\gamma}^t\}_{t=1}^T)$ for attack method $\gamma = \text{FGSM}$ (in %), showing transferability from surrogate model $s \in \mathcal{S} = \{f_{\boldsymbol{\theta}_0}, f_{\boldsymbol{\theta}_t}\}$ to target models \mathcal{T} . $\{\overline{R}_{\gamma}^{t,s}\}_{t=1}^T$ is mean relative transfer ASR.

Task t	$\mathcal{S}\downarrow /\mathcal{T}\rightarrow$	f_{θ_0}	$f_{\boldsymbol{\theta}_t}$	$f_{\theta_{mtl}^{\text{WA}}}$	$f_{\boldsymbol{\theta}_{mtl}^{\mathrm{TA}}}$	$f_{\boldsymbol{\theta}_{mtl}^{\mathrm{TM}}}$	$f_{\boldsymbol{\theta}_{mtl}^{\mathrm{AM}}}$	$f_{\boldsymbol{\theta}_{mtl}^{\text{WA+RS}}}$	$f_{\boldsymbol{\theta}_{mtl}^{\text{TA+RS}}}$	$f_{\boldsymbol{\theta}_{mtl}^{\mathrm{TM+RS}}}$	$f_{\boldsymbol{\theta}_{mtl}^{\text{AM+RS}}}$	$R_{\gamma}^{t, s}$
(t=1) Cars	$\begin{array}{c c} s = f_{\boldsymbol{\theta}_0} \\ s = f_{\boldsymbol{\theta}_t} \end{array}$	76.84 78.21	41.31 89.65	54.12 85.25	47.11 81.98	50.22 85.21	51.83 86.37	53.03 84.85	45.59 80.81	49.04 84.11	50.69 84.82	65.34 93.89
(t=2) MNIST	$\begin{array}{c c} s = f_{\theta_0} \\ s = f_{\theta_t} \end{array}$	96.05 96.05	92.12 90.84	88.90 88.73	85.07 85.93	87.74 88.95	83.38 88.42	86.72 84.70	90.24 88.75	89.34 88.58	83.86 89.14	90.48 96.76
(t=3) EuroSAT	$\begin{array}{c c} s = f_{\boldsymbol{\theta}_0} \\ s = f_{\boldsymbol{\theta}_t} \end{array}$	55.11 55.00	30.30 67.28	49.26 63.83	38.04 60.39	42.70 63.00	48.07 69.59	37.30 62.85	26.80 55.50	37.48 62.63	37.50 61.13	71.94 92.69
(t=4) GTSRB	$\begin{array}{c c} s = f_{\boldsymbol{\theta}_0} \\ s = f_{\boldsymbol{\theta}_t} \end{array}$	80.49 80.65	4.87 44.65	53.88 59.47	35.76 51.33	43.25 54.60	44.60 54.69	37.73 46.88	22.20 39.22	30.63 43.09	32.67 45.05	46.70 110.39
(t=5) SVHN	$\begin{array}{c c} s = f_{\boldsymbol{\theta}_0} \\ s = f_{\boldsymbol{\theta}_t} \end{array}$	99.34 99.37	9.49 54.96	58.08 61.55	34.30 46.23	41.10 49.56	36.75 45.19	46.86 54.61	30.19 44.76	38.88 47.26	37.38 46.52	40.71 89.99
(t=6) RESISC45	$s = f_{\theta_0}$ $s = f_{\theta_t}$	67.54 74.06	17.56 72.86	47.87 71.52	41.33 66.76	45.95 71.67	47.21 72.21	42.43 73.32	31.27 65.05	39.56 72.13	39.29 71.78	61.98 96.84
(t=7) DTD	$\begin{array}{c c} s = f_{\boldsymbol{\theta}_0} \\ s = f_{\boldsymbol{\theta}_t} \end{array}$	19.79 19.04	35.16 67.77	46.01 59.73	39.04 52.55	41.81 56.12	42.98 59.10	41.81 61.54	33.78 53.30	38.09 57.87	38.88 59.31	203.64 84.76

TABLE E.2 ASR matrices ($\{\mathbf{A}_{\gamma}^t\}_{t=1}^T$) for attack method $\gamma=$ I-FGSM (in %), showing transferability from surrogate model $s\in\mathcal{S}=\{f_{\boldsymbol{\theta}_0},f_{\boldsymbol{\theta}_t}\}$ to target models \mathcal{T} . $\{\overline{R}_{\gamma}^{t,s}\}_{t=1}^T$ is mean relative transfer ASR.

Task t	$\mid \mathcal{S}\downarrow /\mathcal{T} \rightarrow$	f_{θ_0}	f_{θ_t}	$f_{\theta_{mtl}^{WA}}$	$f_{m{ heta}_{mtl}^{ ext{TA}}}$	$f_{m{ heta}_{mtl}^{ ext{TM}}}$	$f_{m{ heta}_{mtl}^{ ext{AM}}}$	$f_{m{ heta}_{mtl}^{ ext{WA+RS}}}$	$f_{m{ heta}_{mtl}^{\mathrm{TA+RS}}}$	$f_{\boldsymbol{\theta}_{mtl}^{\mathrm{TM+RS}}}$	$f_{\boldsymbol{\theta}_{mtl}^{\text{AM+RS}}}$	$\overline{R}_{\gamma}^{t, s}$
(t=1) Cars	$\begin{vmatrix} s = f_{\theta_0} \\ s = f_{\theta_t} \end{vmatrix}$	77.75 57.90	62.27 96.08	80.03 95.56	51.81 90.27	67.37 94.49	76.56 95.46	78.06 95.27	49.94 89.76	64.92 94.24	75.10 95.11	87.43 97.60
(t=2) MNIST	$\begin{vmatrix} s = f_{\theta_0} \\ s = f_{\theta_t} \end{vmatrix}$	93.41 94.58	0.07 90.97	16.07 79.14	1.18 57.20	3.08 66.70	0.75 84.14	8.00 74.24	0.73 55.61	1.57 63.20	0.67 84.47	4.29 77.59
(t=3) EuroSAT	$\begin{vmatrix} s = f_{\theta_0} \\ s = f_{\theta_t} \end{vmatrix}$	70.61 61.11	31.24 99.89	79.26 90.70	55.35 93.02	72.33 90.74	63.07 95.30	65.06 97.87	43.19 97.24	58.67 97.78	54.80 97.76	87.05 95.16
(t=4) GTSRB	$\begin{vmatrix} s = f_{\theta_0} \\ s = f_{\theta_t} \end{vmatrix}$	79.37 80.83	5.30 99.27	72.73 93.66	37.46 93.56	54.03 95.00	54.37 94.75	62.12 95.59	24.76 91.46	45.42 95.77	44.99 95.61	62.35 95.12
(t=5) SVHN	$\begin{vmatrix} s = f_{\theta_0} \\ s = f_{\theta_t} \end{vmatrix}$	85.06 98.00	7.10 98.95	70.11 92.37	38.28 94.79	56.35 95.18	52.24 95.95	72.35 94.07	35.70 95.88	54.75 95.99	50.23 96.80	63.19 96.14
(t=6) RESISC45	$\begin{vmatrix} s = f_{\theta_0} \\ s = f_{\theta_t} \end{vmatrix}$	72.29 71.03	30.76 97.10	75.21 92.19	54.25 90.32	67.78 92.08	67.56 92.95	71.95 94.44	44.79 92.89	63.06 94.24	63.90 94.49	87.93 95.73
(t=7) DTD	$\begin{vmatrix} s = f_{\boldsymbol{\theta}_0} \\ s = f_{\boldsymbol{\theta}_t} \end{vmatrix}$	38.99 21.54	45.69 84.63	66.28 82.82	49.47 75.90	59.73 80.48	63.14 82.93	62.13 85.00	42.29 79.04	54.73 83.19	58.19 84.31	146.18 96.55

TABLE E.3 ASR matrices $(\{\mathbf{A}_{\gamma}^t\}_{t=1}^T)$ for attack method $\gamma = \mathrm{PGD}$ (in %), showing transferability from surrogate model $s \in \mathcal{S} = \{f_{\boldsymbol{\theta}_0}, f_{\boldsymbol{\theta}_t}\}$ to target models \mathcal{T} . $\{\overline{R}_{\gamma}^{t,s}\}_{t=1}^T$ is mean relative transfer ASR.

Task t	$\int \mathcal{S} \downarrow / \mathcal{T} \rightarrow$	f_{θ_0}	$f_{\boldsymbol{\theta}_t}$	$f_{\theta_{mtl}^{WA}}$	$f_{m{ heta}_{mtl}^{ ext{TA}}}$	$f_{m{ heta}_{mtl}^{ ext{TM}}}$	$f_{m{ heta}_{mtl}^{ ext{AM}}}$	$f_{m{ heta}_{mtl}^{ ext{WA+RS}}}$	$f_{m{ heta}_{mtl}^{\mathrm{TA+RS}}}$	$f_{m{ heta}_{mtl}^{\mathrm{TM+RS}}}$	$f_{m{ heta}_{mtl}^{ ext{AM+RS}}}$	$\overline{R}_{\gamma}^{t, s}$
(t=1) Cars	$\begin{array}{c c} s = f_{\boldsymbol{\theta}_0} \\ s = f_{\boldsymbol{\theta}_t} \end{array}$	81.89 72.23	76.59 98.00	88.41 97.85	64.84 95.86	79.12 97.56	85.87 97.94	87.49 97.76	62.31 95.91	77.32 97.57	84.39 97.69	96.13 99.26
(t=2) MNIST	$ \begin{vmatrix} s = f_{\theta_0} \\ s = f_{\theta_t} \end{vmatrix} $	95.98 95.39	1.48 99.92	66.52 98.48	18.50 99.35	38.82 99.10	18.32 99.85	52.53 99.53	14.34 99.59	30.65 99.53	18.36 99.86	33.61 99.49
(t=3) EuroSAT	$\begin{vmatrix} s = f_{\theta_0} \\ s = f_{\theta_t} \end{vmatrix}$	66.93 58.70	36.67 99.91	81.56 89.67	58.33 92.33	75.06 90.20	64.96 94.80	66.28 97.69	45.19 97.06	60.87 97.63	56.83 97.74	95.07 94.73
(t=4) GTSRB	$\begin{vmatrix} s = f_{\theta_0} \\ s = f_{\theta_t} \end{vmatrix}$	81.48 81.46	6.31 99.31	73.91 93.50	39.25 93.30	55.59 95.08	57.15 94.79	64.19 95.98	25.64 90.61	46.89 95.95	47.78 96.26	62.96 95.09
(t=5) SVHN	$\begin{array}{c c} s = f_{\boldsymbol{\theta}_0} \\ s = f_{\boldsymbol{\theta}_t} \end{array}$	92.60 98.37	7.51 98.98	74.28 92.38	38.69 94.78	58.28 95.20	53.53 96.14	74.01 94.02	36.67 95.73	55.87 96.00	51.61 96.80	59.80 96.11
(t=6) RESISC45	$\begin{vmatrix} s = f_{\boldsymbol{\theta}_0} \\ s = f_{\boldsymbol{\theta}_t} \end{vmatrix}$	74.08 69.56	30.29 97.43	75.98 92.44	54.83 90.27	68.06 92.38	68.75 93.06	72.98 94.65	44.37 92.78	63.25 94.51	64.79 94.71	86.57 95.56
(t=7) DTD	$\begin{vmatrix} s = f_{\theta_0} \\ s = f_{\theta_t} \end{vmatrix}$	37.77 21.01	45.48 86.86	66.17 82.55	48.56 75.11	59.63 80.00	62.02 82.13	62.23 85.32	43.94 78.03	54.79 83.94	57.82 84.73	150.65 93.81

 $\text{TABLE E.4} \\ \text{ASR MATRICES } (\{\mathbf{A}_{\gamma}^t\}_{t=1}^T) \text{ for attack method } \gamma = \text{TI-FGSM (in \%), showing transferability from surrogate model } s \in \mathcal{S} = \{f_{\boldsymbol{\theta}_0}, f_{\boldsymbol{\theta}_t}\} \\ \text{ to target models } \mathcal{T}. \ \{\overline{R}_{\gamma}^{t,\,s}\}_{t=1}^T \text{ is mean relative transfer ASR.}$

Task t	$\int \mathcal{S} \downarrow / \mathcal{T} \rightarrow$	f_{θ_0}	f_{θ_t}	$f_{\theta_{mtl}^{WA}}$	$f_{m{ heta}_{mtl}^{\mathrm{TA}}}$	$f_{m{ heta}_{mtl}^{ ext{TM}}}$	$f_{m{ heta}_{mtl}^{ ext{AM}}}$	$f_{m{ heta}_{mtl}^{ ext{WA+RS}}}$	$f_{\boldsymbol{\theta}_{mtl}^{\mathrm{TA+RS}}}$	$f_{\boldsymbol{\theta}_{mtl}^{\text{TM+RS}}}$	$f_{\boldsymbol{\theta}_{mtl}^{\text{AM+RS}}}$	$\overline{R}_{\gamma}^{t, s}$
(t=1) Cars	$\begin{vmatrix} s = f_{\theta_0} \\ s = f_{\theta_t} \end{vmatrix}$	59.67 43.70	23.94 88.71	40.08 81.16	24.80 66.60	29.74 76.62	35.57 81.36	38.99 81.27	23.77 67.17	28.89 76.67	35.34 81.22	53.88 86.25
(t=2) MNIST	$ \begin{vmatrix} s = f_{\theta_0} \\ s = f_{\theta_t} \end{vmatrix} $	96.66 96.04	0.16 89.56	21.78 79.98	1.61 71.82	3.77 76.79	1.06 85.54	9.12 77.46	0.98 71.02	2.01 75.21	0.94 85.68	5.34 87.02
(t=3) EuroSAT	$\begin{vmatrix} s = f_{\theta_0} \\ s = f_{\theta_t} \end{vmatrix}$	58.28 52.61	2.93 99.52	37.94 70.48	12.98 61.48	23.43 67.00	18.17 77.70	16.52 84.09	4.87 68.48	10.15 80.31	9.83 84.80	28.72 74.65
(t=4) GTSRB	$\begin{vmatrix} s = f_{\theta_0} \\ s = f_{\theta_t} \end{vmatrix}$	67.11 61.43	0.67 59.79	34.14 58.62	12.57 47.24	18.01 54.73	17.51 53.94	17.91 49.29	5.99 38.72	10.52 45.16	10.25 46.63	23.64 82.44
(t=5) SVHN	$\begin{vmatrix} s = f_{\theta_0} \\ s = f_{\theta_t} \end{vmatrix}$	62.99 81.10	0.90 89.11	23.50 67.89	7.49 63.61	10.60 70.30	10.29 75.00	25.41 70.17	6.70 65.53	10.35 71.60	9.42 77.11	20.59 78.72
(t=6) RESISC45	$\begin{vmatrix} s = f_{\theta_0} \\ s = f_{\theta_t} \end{vmatrix}$	51.73 42.76	4.75 93.71	35.33 79.14	17.87 64.86	25.51 77.13	27.29 77.95	26.51 82.35	12.06 66.19	18.76 79.76	20.87 79.67	44.51 80.97
(t=7) DTD	$\begin{vmatrix} s = f_{\boldsymbol{\theta}_0} \\ s = f_{\boldsymbol{\theta}_t} \end{vmatrix}$	33.83 19.57	12.50 74.68	30.90 49.89	18.46 37.98	24.52 44.20	25.00 51.01	25.74 54.04	13.40 37.87	19.79 49.26	20.74 54.04	65.97 63.32

20

APPENDIX F RESULT ON TARGETED ATTACK

TABLE F.1 ASR matrices $(\{\mathbf{A}_{\gamma}^t\}_{t=1}^T)$ for targeted attack with attack method $\gamma=\text{NI-FGSM}$ (in %), showing transferability from surrogate model $s\in\mathcal{S}=\{f_{m{ heta}_0},f_{m{ heta}_t}\}$ to target models $\mathcal{T}.\{\overline{R}_{\gamma}^{t,s}\}_{t=1}^T$ is relative mean transfer ASR, denoting success of transfer attack.

Task t	$\mid \mathcal{S} \downarrow / \mathcal{T} \rightarrow$	f_{θ_0}	f_{θ_t}	$f_{\boldsymbol{\theta}_{mtl}^{\text{WA}}}$	$f_{m{ heta}_{mtl}^{ ext{TA}}}$	$f_{m{ heta}_{mtl}^{ ext{TM}}}$	$f_{m{ heta}_{mtl}^{ ext{AM}}}$	$f_{m{ heta}_{mtl}^{ ext{WA+RS}}}$	$f_{m{ heta}_{mtl}^{\mathrm{TA+RS}}}$	$f_{m{ heta}_{mtl}^{\mathrm{TM+RS}}}$	$f_{m{ heta}_{mtl}^{ ext{AM+RS}}}$	$\overline{R}_{\gamma}^{t, s}$
(t=1) Cars	$\begin{vmatrix} s = f_{\theta_0} \\ s = f_{\theta_t} \end{vmatrix}$	99.25 0.02	0.07 100.00	0.20 84.90	0.10 68.17	0.15 82.57	0.10 80.33	0.12 87.74	0.07 70.90	0.17 85.72	0.07 85.43	0.12 80.72
(t=2) MNIST	$\begin{vmatrix} s = f_{\theta_0} \\ s = f_{\theta_t} \end{vmatrix}$	99.66 0.06	0.02 100.00	0.22 98.16	0.16 99.90	0.20 99.86	0.18 99.98	0.10 99.56	0.04 99.90	0.08 99.94	0.18 100.00	0.15 99.66
(t=3) EuroSAT	$\begin{vmatrix} s = f_{\theta_0} \\ s = f_{\theta_t} \end{vmatrix}$	77.48 0.00	0.04 99.59	0.11 88.81	0.07 86.70	0.11 89.48	0.11 83.26	0.07 81.59	0.04 80.19	0.04 83.33	0.04 78.67	0.10 84.35
(t=4) GTSRB	$\begin{vmatrix} s = f_{\theta_0} \\ s = f_{\theta_t} \end{vmatrix}$	96.77 0.02	0.06 96.03	0.19 56.50	0.16 59.79	0.13 62.11	0.14 51.51	0.11 50.17	0.17 52.92	0.11 58.13	0.10 48.22	0.14 57.19
(t=5) SVHN	$\begin{vmatrix} s = f_{\theta_0} \\ s = f_{\theta_t} \end{vmatrix}$	83.26 0.01	0.03 99.75	0.22 81.23	0.12 94.58	0.18 95.33	0.11 95.27	0.14 83.77	0.08 94.30	0.12 95.09	0.09 96.39	0.16 92.23
(t=6) RESISC45	$\begin{vmatrix} s = f_{\theta_0} \\ s = f_{\theta_t} \end{vmatrix}$	93.94 0.00	0.06 100.00	0.29 89.65	0.22 78.16	0.25 89.68	0.19 83.08	0.29 90.83	0.22 80.41	0.25 91.37	0.19 87.78	0.25 86.37
(t=7) DTD	$\begin{vmatrix} s = f_{\theta_0} \\ s = f_{\theta_t} \end{vmatrix}$	74.68 0.00	0.11 98.72	0.00 68.40	0.11 43.51	0.11 63.09	0.11 61.81	0.00 74.47	0.11 48.30	0.00 69.26	$0.11 \\ 71.17$	0.09 63.31

APPENDIX G RESULT ON RESNET-50 SURROGATE

TABLE G.1 ASR matrices $(\{\mathbf{A}_{\gamma}^t\}_{t=1}^T)$ for attack method $\gamma=$ NI-FGSM (in %), showing transferability from ResNet-50 surrogate model $s\in\mathcal{S}=\{f_{\theta_0}^r,f_{\theta_t}^r\}$ to target models $\mathcal{T}.$ $\{\overline{R}_{\gamma}^{t,s}\}_{t=1}^T$ is relative mean transfer ASR, denoting success of transfer attack.

Task t	$\int \mathcal{S} \downarrow / \mathcal{T} \rightarrow$	$f_{\boldsymbol{\theta}_0}^r$	$f_{m{ heta}_t}^r$	$f_{\theta_{mtl}^{WA}}$	$f_{m{ heta}_{mtl}^{ ext{TA}}}$	$f_{m{ heta}_{mtl}^{ ext{TM}}}$	$f_{m{ heta}_{mtl}^{ ext{AM}}}$	$f_{m{ heta}_{mtl}^{ ext{WA+RS}}}$	$f_{m{ heta}_{mtl}^{\mathrm{TA+RS}}}$	$f_{\boldsymbol{\theta}_{mtl}^{\mathrm{TM+RS}}}$	$f_{\boldsymbol{\theta}_{mtl}^{\text{AM+RS}}}$	$R_{\gamma}^{t, s}$
(t=1) Cars	$\begin{array}{c c} s = f^r_{\boldsymbol{\theta}_0} \\ s = f^r_{\boldsymbol{\theta}_t} \end{array}$	71.05 77.05	25.79 35.46	35.74 44.29	42.38 50.14	35.04 44.17	32.65 44.42	35.64 45.21	39.72 48.40	34.79 43.99	34.20 44.59	51.05 128.74
(t=2) MNIST	$\begin{array}{c c} s = f^r_{\boldsymbol{\theta}_0} \\ s = f^r_{\boldsymbol{\theta}_t} \end{array}$	96.38 96.40	0.52 43.06	20.16 65.12	5.48 36.70	6.92 47.26	1.50 33.78	10.12 63.90	2.98 33.98	4.00 44.52	1.26 31.84	6.80 103.66
(t=3) EuroSAT	$\begin{array}{c c} s = f^r_{\boldsymbol{\theta}_0} \\ s = f^r_{\boldsymbol{\theta}_t} \end{array}$	42.89 48.67	67.63 78.37	64.41 79.07	73.67 79.22	67.52 78.70	64.52 75.04	47.00 74.48	59.63 69.85	51.63 76.63	59.63 75.70	142.23 97.09
(t=4) GTSRB		80.41 80.63	20.46 39.11	55.22 66.14	49.25 63.09	48.52 62.25	46.43 63.06	46.92 62.99	40.70 54.71	43.15 58.53	41.19 57.24	57.73 155.97
(t=5) SVHN		99.33 99.48	11.60 64.01	43.63 59.96	47.34 56.98	39.26 63.09	35.14 66.53	44.65 66.79	39.66 59.00	37.75 61.36	33.68 66.79	40.41 97.74
(t=6) RESISC45		45.11 60.25	54.57 82.41	47.46 74.98	58.03 75.87	47.08 73.21	51.43 76.51	46.86 78.29	59.59 78.70	46.16 74.83	50.19 76.22	112.72 92.31
(t=7) DTD	$\begin{vmatrix} s = f_{\theta_0}^r \\ s = f_{\theta_t}^r \end{vmatrix}$	19.15 18.83	28.51 36.91	41.28 44.79	43.94 48.19	38.72 43.40	35.74 40.74	41.28 46.38	46.91 51.06	38.72 43.30	37.98 43.83	211.86 122.49

APPENDIX H RESULT ON QUERY-BASED (BLACK-BOX) ATTACK

TABLE H.1 ASR (%) FOR Square Attack across target models on each dataset.

Dataset	f_{θ_0}	$f_{\boldsymbol{\theta}_t}$	$f_{\boldsymbol{\theta}_{mtl}^{\text{WA}}}$	$f_{m{ heta}_{mtl}^{ ext{TA}}}$	$f_{m{ heta}_{mtl}^{ ext{TM}}}$	$f_{m{ heta}_{mtl}^{ ext{AM}}}$	$f_{\boldsymbol{\theta}_{mtl}^{\text{WA+RS}}}$	$f_{m{ heta}_{mtl}^{\mathrm{TA+RS}}}$	$f_{m{ heta}_{mtl}^{\mathrm{TM+RS}}}$	$f_{m{ heta}_{mtl}^{ ext{AM+RS}}}$
Cars	84.08	90.05	95.00	92.50	85.00	92.50	90.00	90.00	95.00	85.00
MNIST	96.80	81.20	96.00	96.00	96.00	96.00	96.00	100.00	94.00	94.00
EuroSAT	47.78	93.70	81.48	85.19	88.89	100.00	100.00	96.30	100.00	100.00
GTSRB	79.24	61.33	87.30	90.48	93.65	95.24	92.06	76.19	88.89	84.13
SVHN	97.62	83.01	82.31	82.31	84.62	88.46	80.00	86.92	84.62	95.38
RESISC45	65.40	90.16	83.87	64.52	74.19	70.97	83.87	77.42	83.87	83.87
DTD	28.72	77.66	66.67	55.56	77.78	55.56	55.56	55.56	66.67	66.67